Title

Mantle helium along the Newport-Inglewood fault zone, Los Angeles basin, California-A leaking paleo-subduction zone

Authors

Boles, J. R
Garven, G.
Camacho, H.
et al.

Publication Date

2015-06-01

DOI

10.1002/2015GC005951

Peer reviewed

Mantle Helium Along the Newport-Inglewood Fault Zone, Los Angeles Basin, California -- A Leaking Paleo-Subduction Zone

J. R. Boles[1], G. Garven[2,] H. Camacho[3], and J. E. Lupton[4]

[1] *J. R. Boles, Department of Earth Science, UCSB, Santa Barbara, CA 93106*

[2] *G. Garven, Department of Earth and Ocean Sciences, Tufts Univ., Medford, MA 02155*

[3] *H. Camacho, Occidental Oil and Gas Corporation, Houston, TX 77046*

[4] *J. E. Lupton, NOAA Pacific Marine Environmental Laboratory, Newport, OR 97365*

Corresponding author:

James Boles, Dept. of Earth Science, Webb Hall, Univ. Calif. Santa Barbara, Santa Barbara, CA 93106. e-mail: boles@geol.ucsb.edu

ABSTRACT

Mantle helium is a significant component of the helium gas from deep oil wells along the Newport-Inglewood fault zone (NIFZ) in the Los Angeles (LA) basin. Helium isotope ratios are as high as 5.3 Ra (Ra=^{3}He/^{4}He ratio of air) indicating 66% mantle contribution, (assuming R/Ra = 8 for mantle), and most values are higher than 1.0 Ra. Other samples from basin margin faults and from within the basin have much lower values (R/Ra < 1.0). The ^{3}He enrichment inversely correlates with CO_2, a potential magmatic carrier gas. The $\delta^{13}C$ of the CO_2 in the ^{3}He rich samples is between 0 and -10 ‰, suggesting a mantle influence. The strong mantle helium signal along the NIFZ is surprising considering that the fault is currently in a transpressional rather than extensional stress regime, lacks either recent magma emplacement or high geothermal gradients, and is modeled as truncated by a proposed major, potentially seismically active, décollement beneath the LA basin. Our results demonstrate that the NIFZ is a deep-seated fault directly or indirectly connected with the mantle. Based on a 1-D model, we calculate a maximum Darcy flow rate $q \sim 2.2$ cm/yr and a fault permeability $k \sim 6 \times 10^{-17}$ m^2 (60

microdarcys), but the flow rates are too low to create a geothermal anomaly. The mantle leakage may be a result of the NIFZ being a former Mesozoic subduction zone in spite of being located 70 km west of the current plate boundary at the San Andreas fault.

1 INTRODUCTION

For crustal fluids, ^{3}He enrichment relative to ^{4}He is the principal indicator of mantle degassing [*Lupton,* 1983] and the $^{3}He/^{4}He$ ratio is a measure of the proportion of mantle-derived ^{3}He mixed with continental derived ^{4}He. Mantle ratios as indicated by mid-ocean ridge basalt (MORB) values are generally 8 Ra (where $R = {}^{3}He/{}^{4}He$ and $Ra = R_{air} = 1.4 \times 10^{-6}$) or higher [*Lupton,* 1983*; Lowenstern et al*., 2014] and recent studies indicate old subcontinental lithospheric mantle values may be as low as 6 Ra [*Gautheron and Moreira*, 2002]. Continental crustal values are about 0.02 Ra due to abundance of ^{4}He from U-Th decay [*Andrews,* 1985]. Areas of continental crust with high mantle He values have been identified, but without evidence of recent magmatism [*Welhan et al*., 1979*; Lupton*, 1983*; Oxburgh et al.*, 1986*; Kennedy and van Soest*, 2007]. These areas are characterized by Cenozoic crustal extension and shear that has been hypothesized as maintaining permeable pathways from the mantle to the crust. Tectonically active major strike-slip faults have been found with high (>13%) mantle component (i.e. R/Ra >1.0) including the North Anatolian Fault in Turkey [*Gülec et al*., 2002], the Karakoram fault in Tibet [*Klemperer et al*., 2013], and the Niigata-Kobe tectonic zone in Japan [*Umeda et al.*, 2013], although most of the He values in these areas have less than 13% mantle component. In addition, most of these areas have elevated heat flow as indicated by hot springs at the surface.

The Newport-Inglewood fault zone (NIFZ) is one of the oldest and most westward faults that is part of the San Andreas fault system (SAFS) in California (Figure 1). The SAFS is a 1300 km strike-slip fault system, considered to be the most seismically active fault in the U.S. that developed in the early Miocene from a subduction zone, which was believed to be near or at the NIFZ [*Wallace*, 1990]. The San Andreas fault forms a single trace in Northern California, but in southern California multiple strands are considered part of the SAFS, including the NIFZ (Figure 1).

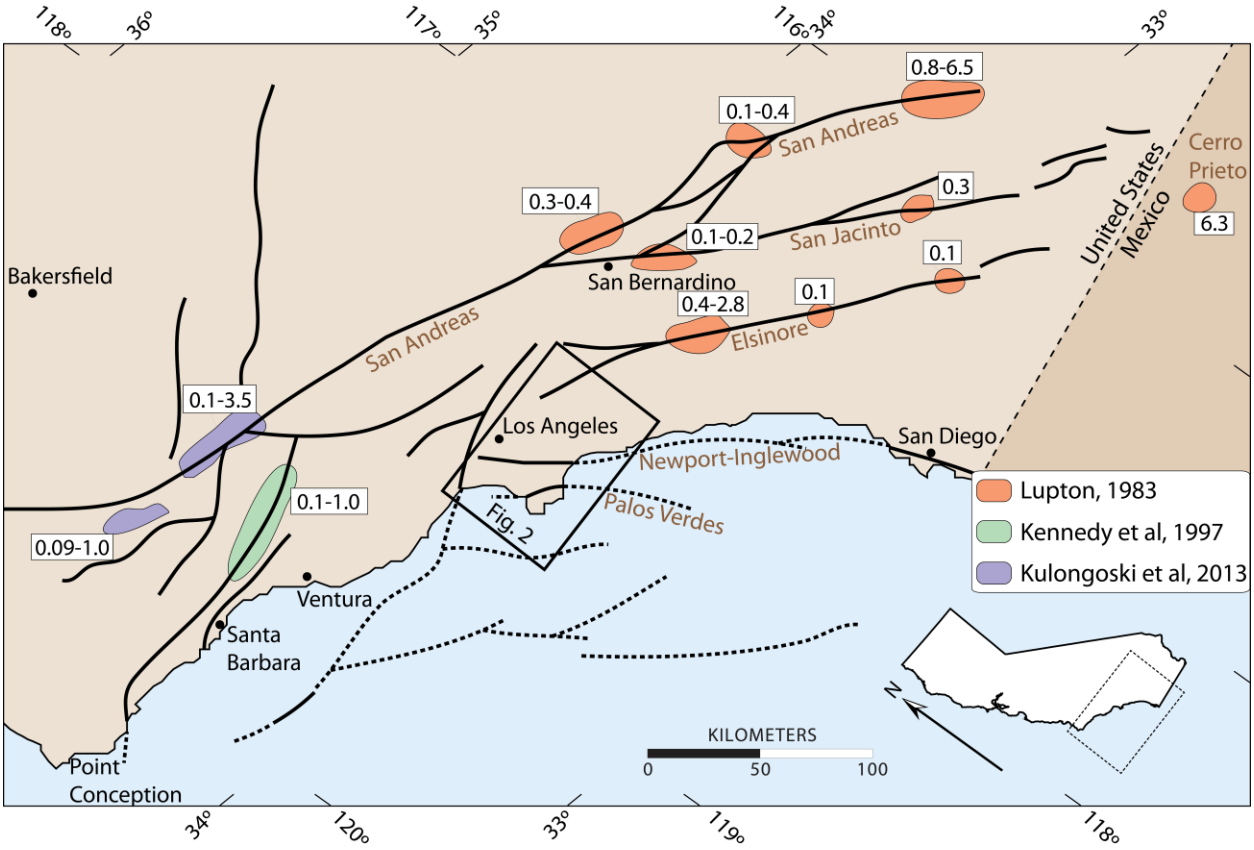

Figure 1. Fault map of southern California showing location of previous He isotopic studies and location of current study in the LA basin (Fig 2). Numbers are the range of R/Ra values from studies of Lupton [1983], Kennedy et al. [1997], and Kulongoski et al. [2013].

The San Andreas fault (SAF) proper, which is the current boundary between the Pacific and North American plates, has highly variable helium isotopic values from approximately 0.1 Ra to 6.5 times Ra $^{3}He/^{4}He$ values [*Lupton*, 1983*; Kennedy et al*., 1997*; Kulongoski et al*., 2013*; Wiersberg and Ezinger*, 2007], indicating varying degrees of mantle contribution along the length of the fault (Figure 1). Some of the highest values are found in the Salton Sea area (Figure 1), which is the southernmost part of the SAF, adjacent to the Gulf of California spreading center. Several geothermal or CO_2 wells in the area have R/Ra values exceeding 6.0 [*see Welhan and others*, 1979*;* Figure 10 in *Lupton*, 1983]. Areas north of the Salton Sea have been shown to have values not exceeding 0.44 Ra, [*Lupton*, 1983]. More recently, a few values as high as R/Ra=3.47 have been recorded on the SAF in the Big Bend area from groundwater well samples [*Kulongoski et al*., 2013]. Further north, of the Big Bend area, the highest values are not on the main strike-slip segment but from hot springs on a fault strand in serpentinite, some 35 km to the east of the SAF [*Kennedy et al*., 1997]. A relatively high 2.8 Ra is reported from Murrieta Hot Springs, approximately 75 km west of Newport Beach, from a sample close to the Elsinore fault and another nearby sample from a thermal spring was R/Ra=0.72 [*Lupton*, 1983]. Clearly there is a lot of variability in mantle-crust communication along the SAF. There are no previous studies of He isotopes within the deep LA basin.

The LA basin encompasses 3200 km^2 with over 17 million people (Figure 1). The area is seismically active [*Hauksson*, 1987], with the most recent major event being the 1994 Northridge earthquake (M_W = 6.7). There is considerable concern about the earthquake potential of blind thrusts in the basin [*Davis et al*., 1989; *Shaw and Suppe*, 1996] and a current USGS and California Division of Mines and Geology mapping initiative will improve our understanding of the seismic risk of the faults in the LA basin. Helium isotopic studies may be important to

evaluate the role of mantle versus metamorphic fluids to fault weakening and seismicity [*Kennedy et al*., 1997*; Gülec et al.*, 2002*; Umeda and Ninomiya*, 2009*; Umeda et al*., 2013]. Evidence that the NIFZ has been a major pathway for fluid movement in the upper crust is the abundance and large vertical distribution of hydrocarbons along the NIFZ, largely generated and trapped within the last five to ten million years [*Wright*, 1991*; Hunt*, 1995*; Jung et al*., 2015]. As shown in this paper, He isotopes suggest that the lower crust is also a pathway from the mantle along the same fault.

The NIFZ has been a major structural feature of the LA basin since at least early Miocene time [Wright, 1991]. The fault zone extends southeast for approximately 65 km from the Santa Monica Mountains to Newport Beach, where it continues offshore [Figure. 1; *Harding*, 1973]. At the surface, the fault is series of left-stepping fault segments, characterized by oblique right slip and associated anticlinal hills. The NIFZ has a relatively small slip rate (0.5cm/year) compared to faults directly eastward (Elsinore fault = 0.5 to 1.0 cm/year; San Jacinto fault = 1.0 to 2.0 cm/year; San Andreas fault = 2.0 to 3.0 cm/year). [see fault locations in Figure 1; *Wallace*, 1990]. In spite of the low slip rate, five earthquakes of magnitude 4.9 or greater have occurred on the fault since 1920, the largest being the M_L = 6.4 Long Beach earthquake of 1933 [*Hauksson*, 1987]. Most earthquakes occur from 6 to 11 km depth, within the 28 to 30 km thick crust. Currently, the regional principal stress in the basin is north-south [*Heidbach et al*., 2008] indicating the NIFZ is undergoing transpressional deformation.

The NIFZ zone separates blueschist basement on the southwest from meta-igneous basement rocks to the northeast and largely based on this, it has been proposed as a compressed Mesozoic subduction zone between Pacific and North American plates [*Hill*, 1971*; Wright*, 1991]. Little is known about the pre-SAFS history (pre-Miocene) of the LA basin, but it is clear

that the NIFZ was in the vicinity of this subduction zone about 30 m.y.b.p. (e.g. see *Wallace*, 1990). Miocene transpression and rotation of blocks has resulted in thinning of the crust [*Nicholson et al*., 1994], and deposition of more than 8 km of Miocene and younger sediment in the central part of the LA basin [*Wright*, 1991]. Mid–Miocene volcanism occurs as a result of crustal thinning along the basin bounding faults, including some areas along the NIFZ. Our helium results suggest the NIFZ has retained a strong connection into the mantle, in spite of complex deformation and an 80 km eastward shift in the Pacific plate boundary to the present SAF [*Wright*, 1991].

In this study, we report numerous high $^3He/^4He$ ratios (R/Ra=1.0 to 5.3) along the NIFZ, which is considered the western most part of the SAFS. The NIFZ is more than 80 km from the main trace of the San Andreas fault, more than 140 km from the Big Bend area, and between 90 and 230 km from the high He anomalies reported by *Welhan et al.* [1979] and *Lupton* [1983] in the Salton Sea area (Figure 1). After a discussion of the isotope data, we develop a 1-D mathematical model for helium mass transport to calculate fluid flow rates in the fault zone using the R/Ra data, explore the coupled effects of fluid flow on heat transport in the LA basin, and calculate fault permeability.

2 SAMPLES

Helium samples were collected from active producing oil wells in stainless steel 500 cc to 1000 cc vessels (Table 1). The gas gauge pressure at the casing gas ports of these wells was 0.034 to 1.38 MPa (5-200 psi) greater than STP. The gases are mostly methane with some $\geq C_2$ gases and minor CO_2 that has degassed from the hydrocarbons and formation water at the perforation interval. At the NOAA laboratory in Newport, Oregon, the gas samples were sub-

sampled into glass ampoules, and then subsequently analyzed for helium isotopes, and He and Ne concentrations on a 21-cm dual-collector mass spectrometer specially designed for helium isotope measurements. Splits of the samples archived in glass ampoules were analyzed for $\delta^{13}C$ and CO_2 concentration by Marvin Lilley at ETH in Zurich, Switzerland. We have also sampled the produced fluids associated with a number of these gases and these will be described in a later paper. The producing intervals are the deepest available production in each area (generally greater than 2 km) and are mainly from mid- to upper-Miocene sandstone, siltstone, and shale. These deep production zones have not been subjected to the fluid injection common to the shallow producers in the basin. Most helium isotopic studies sample surface fluids from springs or groundwater wells [e.g. *Oxburgh et al.,* 1986*, Gülec et al.,* 2002*; Du et al.,* 2006*; Kennedy and van Soest*, 2007*; Umeda and Ninomiya*, 2009*; Kulongoski et al*., 2013]. The advantage of deep well sampling is surface air contamination is generally not a problem, as the flux is principally vertical as opposed to potential lateral flow from groundwater movement, and there is a subsurface geologic context for the fluids. The disadvantage is limited numbers of costly (greater than $1M USD) deep wells for sampling, gaining access to regulated industrial sites, and shipping pressurized flammable gas for analysis.

Table 1. Gas samples from Miocene sediments of the LA basin

Samples arranged approximately north to south. C = commingled. Figure 2 shows sample locations.

Sample	Oil Field	Well ID	Lat	Long	Sample Date	Mean Sample Depth (km)	Perf interval (km)	Temp °C
1	Sawtelle (SW)	OF15-RD1	34.0586	-118.4567	1/8/12	3.53	0.27	122
2	Beverly Hills (BH)	WP11RD2	34.0556	-118.3905	24/4/14	2.51	0.56	84
3	Sansinena (S)	12A-5	33.9570	-117.9680	12/2/14	1.15	0.20	44-49
4	Sansinena (S)	4H-53	33.9627	-117.9650	12/2/14	1.01	0.27	51-61
5	Santa Fe Springs (SF)	C	33.9429	-118.0672	1/1/13	1.93	2.03	47 - 100
6	Inglewood (I)	VIC-1-935	34.0057	-118.3765	1/8/12	2.80	0.06	93-107
7	Inglewood (I)	VIC-1-845	34.0057	-118.3765	1/8/12	2.58	0.14	93-107
8	Dominguez (D)	Dominguez #1	33.8635	-118.2432	12/2/14	2.45	0.82	102-129
9	Dominguez (D)	Dominguez #2	33.8635	-118.2431	12/2/14	3.73	0.24	151
10	Long Beach Airport (LBA)	LBA-1	33.8185	-118.1665	11/2/14	2.75	0.45	120
11	Long Beach Airport (LBA)	C-37	33.8100	-118.1709	18/6/14	2.56	0.36	116
12	Long Beach (LB)	B-14	33.8113	-118.1802	1/8/12	2.37	0.34	102-109
13	Long Beach (LB)	B-14	33.8113	-118.1802	11/2/14	2.37	0.34	102-109
14	Long Beach (LB)	23-25	33.8021	-118.1650	24/4/14	3.57	0.31	153
15	Long Beach (LB)	D-81	33.8057	-118.1703	18/6/14	3.56	0.30	154
16	Long Beach (LB)	ALA-49A	33.7993	-118.1568	11/2/14	2.31	0.60	80-85
17	Long Beach (LB)	A-59	33.8126	-118.1825	18/6/14	3.68	1.03	166
18	Wilmington (W)	C-348	33.7393	-118.1387	22/4/14	3.06	0.06	167
19	Belmont (BL)	C-236	33.7395	-118.1383	22/4/14	0.93	0.06	89
20	Huntington Beach (HB)	N. Bolsa	33.7027	-118.0238	12/2/14	1.37	0.30	51-86
21	Huntington Beach (HB)	HB A001	33.6627	-118.0448	12/2/14	0.33	0.09	31
22	Beta Field (B)	B-20	33.5957	-118.1416	30/1/14	0.76	0.30	42
23	Newport Beach (NB)	Commingled	33.6260	-117.9463	24/4/14	1.07	0.50	43

Table 2. Isotopic and CO_2 content of gas samples from Miocene sediments of the LA basin.

See Table 1 and Figure 2 for sample locations. Newport-Inglewood fault zone (NIFZ) shown in Figure 2.

Sample	Distance to NIFZ (km)	R/Ra*	Rc/Ra**	ppmv He	He/Ne/air	$He/^{36}Ar$/air	CO_{2}*** mole %	$\delta^{13}C\ CO_{2}$**** (+/- 0.17)	Lab
1	6	0.324	0.322	8.5		256	2.38		LLBL
2	1	0.721	0.720	5.63	1122		2.01-0.85		NOAA
3	26.2	0.154	0.117	0.829	23.67		2.47 ★	17.63	NOAA
4	26.8	0.144	0.135	0.531	94.4		8.8 ★	16.13	NOAA
5	17.2	0.301	0.177	2.25		7.2	6.84-0.93		USGS
6	0	1.875	1.88	7.20		81	ND		LLBL
7	0.5	2.273	2.28	5.71		94	ND		LLBL
8	0	3.58	3.58	5.58	1344		0.95 ★	-0.22	NOAA
9	0	5.30	5.31	13.1	1208		1.21 ★	-10.64	NOAA
10	1	4.05	4.06	1.6	632		0.26 ★	-8.21	NOAA
11	0	3.06	3.18	5.63	17.73		2.15		NOAA
12	0	3.065	3.07	6.96		80	ND		LLBL
13	0	3.62	3.62	9.62	1403		0.57 ★	-10.87	NOAA
14	0	0.537	0.537	17.9	1556		ND		NOAA
15	0	0.553	0.552	7.33	596		9.45		NOAA
16	0.2	1.09	1.09	3.96	1028		1.74 ★	1.96	NOAA
17	0	1.48	1.48	19.1	2729		8.02		NOAA
18	4	0.105	0.105	17.7	3024		ND		NOAA
19	3.6	0.561	0.549	0.380	37.8		ND		NOAA
20	1.8	2.81	2.81	7.41	934		5.20 ★	-1.34	NOAA
21	4	0.527	0.527	2.67	665		1.78 ★	16.00	NOAA
22	12.2	0.897	0.897	1.41	444		2.53 ★	10.54	NOAA
23	0	0.111	0.104	4.33	134.4		2.41-2.48		NOAA

* Helium isotope ratio, $R = {}^{3}He/{}^{4}He$ and $Ra = Rair = 1.4 \times 10^{-6}$

** Helium isotope ratio corrected for atmospheric helium addition using the formula:

Rc/Ra =((R/Ra) X - 1)/(X-1) where X = (He/Ne)/(He/Ne)air or X = (He/36Ar)/(He/36Ar)air

*** Values with star symbol ★ determined on helium sample by Marvin Lilley, U of Washington.

(Other values are from produced gas analysis reports)

**** Determined by Marvin Lilley, U of Washington

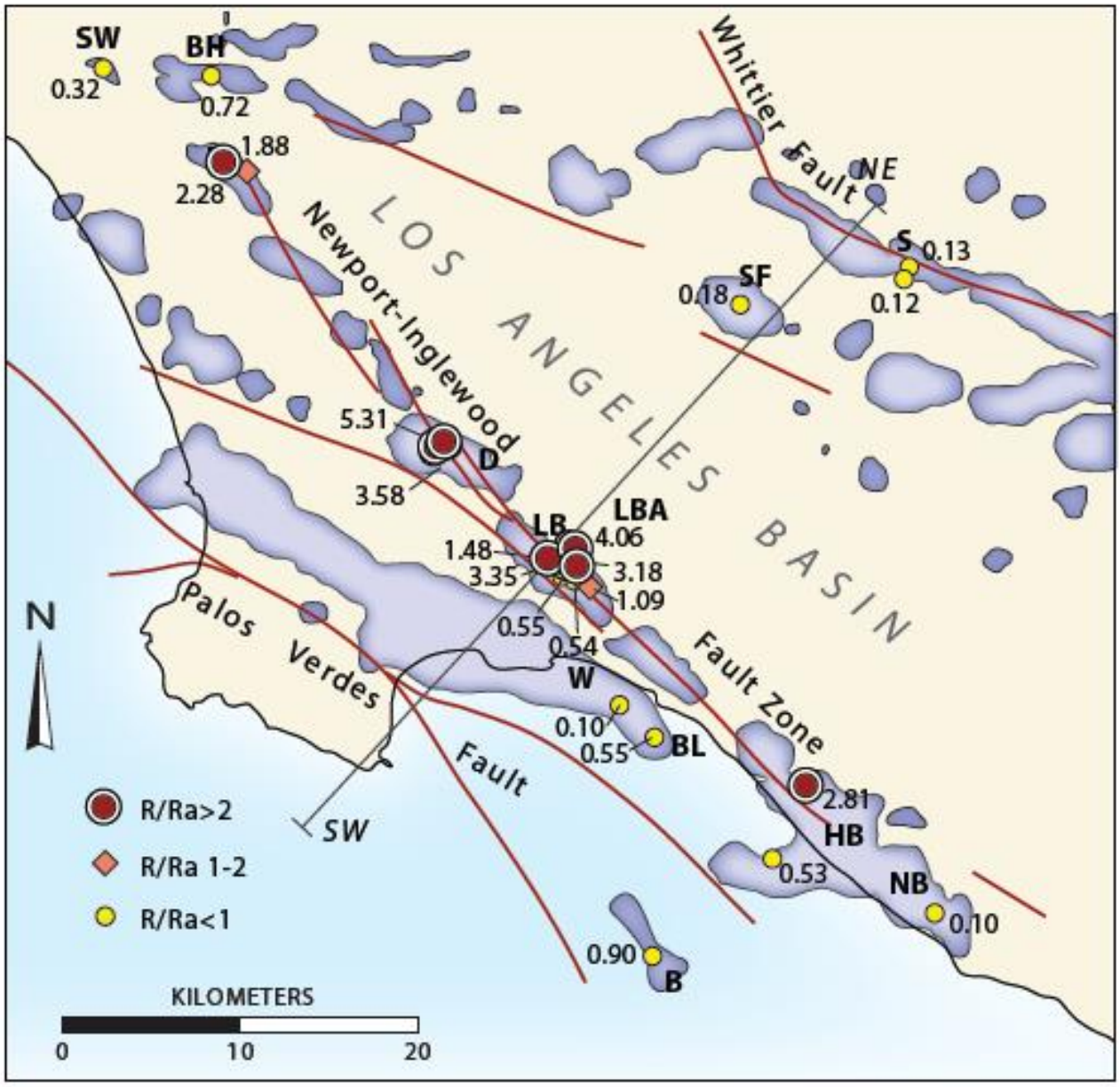

Figure 2. Map of Los Angeles basin and the Newport Inglewood fault zone (NIFZ) showing high Rc/Ra values of most samples along the NIFZ. Numbers are Rc/Ra helium isotope values of sampled wells (purple areas are oil fields). See Figure 1 for map location. Oil fields abbreviations are: B (Beta), BH (Beverly Hills), BL (Belmont), D (Dominguez), HB (Huntington Beach), I (Inglewood), LB (Long Beach), LBA (Long Beach Airport), NB (Newport Beach), S (Sansinena), SF (Santa Fe Springs), SW (Sawtelle), and W (Wilmington). Wells identification numbers and supporting data are given in Table 1. Cross section line across the NIFZ from the Whittier fault (northeast NE) to the Palos Verdes fault (southwest SW) is shown in Figure 7.

3 RESULTS

The $^{3}He/^{4}He$ ratios in Table 2 are given both as R/Ra, which is the empirical or measured value, and as Rc/Ra, which is the ratio corrected for atmospheric helium contamination. The correction is based on the He/Ne or He/Ar ratios in the samples, assuming that the Ne and Ar are atmospheric in origin. The He/Ne ratios and He/Ar ratios indicate that the samples have minimal atmospheric contamination, which is consistent with little or no injection of surface water in these deep wells. Only two samples, Santa Fe Springs and Sansinena Well 12-5 required significant air correction (Table 2).

High Rc/Ra values along the NIFZ compared with other areas in the basin are obvious in Figure 2, with values exceeding ~3Ra being common (Table 2). The affinity of the NIFZ helium with mantle helium is clear (Figures 2 and 3).

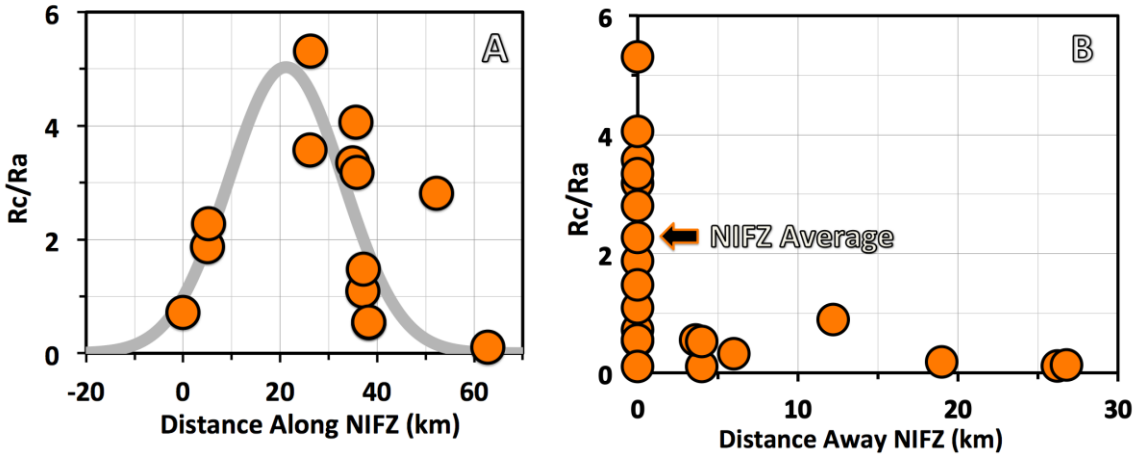

Figure 3. Rc/Ra values of this LA basin study (orange dots) relative to distance along (Figure 3A), and away from the NIFZ (Figure 3B). The dashed curve in Fig 3A shows a best-fit regression of the data to a normal probability density function with spatial mean 21.2 km and standard deviation 11.8 km. The average of all values on the NIFZ is Rc/Ra =2.2. The San Andreas fault values along the Mission Creek segment [Lupton, 1983] and the Big Bend segment [Kulongoski et al., 2013] are generally lower than the NIFZ values from our study and average ~1.0 (see Figure 1). In Fig 3A, the Beverly Hills oil field position (see Figure 2) provides the arbitrary reference point for x =0 km for distance along the NIFZ.

The highest value (5.3 Ra) indicates up to 66% mantle contribution to the He gas (assuming upper mantle helium averages 8 Ra). The Rc/Ra values appear to fit a Gaussian spatial trend along the NIFZ (Figure 3A), suggesting, perhaps, the possibility of a discrete source at the base of the crust. More samples would be required to confirm this. A number of shallow samples tend to have low R/Ra values whereas deep samples tend to have higher R/Ra values, which we interpret as an overprint of in situ produced crustal ^{4}He added to the shallower samples. However, deep samples (e.g. compare Sawtelle, Wilmington, Dominguez and Long Beach field samples of Table 1) have considerable variability in R/Ra values, which indicate that there are real differences in fractions of mantle verses crustal helium within the deep basin.

Although the casing gas is principally methane with some heavier hydrocarbons, the CO_2 content of the sampled gas has a wide range of values (see Table 2; 0.5 to more than 9 mole percent CO_2). CO_2 is believed to be a carrier gas for mantle helium [*Marty and Jambon*, 1987], and the origin of the CO_2 will be discussed in a later section of the paper.

The helium content of the ^{3}He-enriched samples is no greater than that in the ^{3}He poor samples, indicating that the strong mantle signature is not correlated with helium abundance (Table 2). We interpret the variation in helium content of the samples to largely be a result of variation in ^{4}He production in the crust due to U and Th heterogeneity. The helium content of gas from Well B-14 (Table 1, Table 2), which was sampled twice (18 month interval), dropped approximately 40% indicating significant variability in the amount of helium over time.

4 DATA ANALYSIS

4.1 Unexpected Helium Anomaly

The conspicuous mantle He enrichment along the NIFZ is unexpected compared to most other areas of continental crust with a mantle helium anomaly. First, the fault is in a transpressional rather than an extensional stress regime, thus faults would be expected to be overall sealing [*Oxburgh et al*., 1986*; O'Nions and Oxburgh*, 1988*; Kennedy and van Soest*, 2007]. A number of recent studies, however, have shown strike-slip faults or faults within the vicinity of active strike-slip faults may have variable but local high mantle helium anomalies in California [*Kennedy at al*., 1997*; Kulongoski et al*., 2013], in Tibet [*Klemperer et al*., 2013], in Turkey [*Gülec et al*., 2002], and in Japan [*Umeda and Ninomiya*, 2009]. In the case of Japan, reduced mantle helium leakage has been noted along thrust versus strike-slip components of faults [*Umeda et al*., 2013]. Presumably discontinuous dilation segments along these faults could provide localized fluid pathways to the lower crust. We find high R/Ra values (R/Ra >1.0 to 5.3) in most of the samples we have collected along the NIFZ, rather than in localized isolated areas along the fault or away from the main fault zone, suggesting the fault is a major conduit to the lower crust.

Second, there is no evidence for recent magmatism in the LA basin. Early-mid Miocene igneous activity from crustal extension is common along the NIFZ [*Wright*, 1991], but other faults in the basin, without strong mantle signatures, had similar igneous activity (e.g. Sansinena field samples of Table 1, along the Whittier fault; see *Bjorklund, 2003*). Thus, the mantle signature does not appear to be related to the presence of Miocene igneous rocks or their deformation in the LA basin. In addition, mantle helium is believed to be largely degassed during igneous emplacement and cooling at time scales less than one to ten million years

[*Kamensky and others*, 1990]. For example, in the Sacramento gas field, high R/Ra values are associated with Pleistocene volcanism [*Poreda et al*., 1986*; Jenden et al*., 1988]. However, in the LA basin, the high Rc values should not be due to *early-mid Miocene* igneous activity.

Third, most mantle helium anomalies are associated with locally elevated thermal gradients such as hot springs, geothermal anomalies, with or without recent volcanism [*see Polyak and Tolstikhin*, 1985*; Oxburgh and O'Nions*, 1987*; Torgersen*, 1993*; Umeda et al*., 2007]. However, exceptions of strong mantle helium anomalies without correlation with surface spring temperature have been observed in some areas including the Sichuan earthquake zone of southwestern China [*Du et al*., 2006], along faults of the Itoigawa-Shizuoka tectonic line in Japan [*Umeda et al*., 2013], and along the North Anatolian Fault Zone of Turkey [*e.g. Gülec et al*., 2002]. In the Big Bend area of the San Andreas fault, the highest value reported (R/Ra = 3.5) is apparently not associated with a hot spring [*Kulongoski et al*., 2013]. The high R/Ra helium values (without the associated heat) could be explained, in most cases, by the unknown circulation path of shallow groundwater. In the case of our field study, the lack of a strong thermal signature is more difficult to explain, as we are sampling at depths where complex meteoric fluid circulation paths cannot be invoked. The fact is that, worldwide, most strong mantle helium anomalies are associated with surface hot springs.

The LA basin has a relatively average crustal geothermal gradient of about 32°C/km [*Price et al*., 1999]. The central syncline, with the thickest sedimentary section, is typically about 28°C/km, whereas the Wilmington area, with relatively thin sedimentary crust, has a relatively high gradient of 55°C/km. The thermal gradient along the NIFZ is about 33°C/km, only slightly elevated compared to other areas in the basin [*Price et al*., 1999]. This is a

surprisingly low value considering the strength of the mantle helium signature at numerous localities (Figure 2).

From the previous considerations, there is no reason to suspect that the NIFZ would be a pathway for substantial mantle degassing along its length. The NIFZ R/Ra values are higher than observed along much of the SAF (Figure 3, average NIFZ R/Ra = 2.2; average SAF R/Ra = 1.0), the current boundary between the Pacific and North American plates. R/Ra values along the much of the SAF are between 0.4 and 2.0 [*Lupton*, 1983*; Kennedy et al*., 1997*; Wiersberg and Erzinger*, 2007]. The highest SAF values are in the crustal shortened Big Bend segment of the fault, an area of transpression, where R/Ra values are between 1.0 and 3.5 (Figure 1, *Kulongoski et al*., 2013), similar to values we observe along the NIFZ, which is approximately 140 km to the southeast of the Big Bend area. It's is interesting to note that in the vicinity of the Big Bend segment of the SAF, the fault dip at deep crustal levels is vertical [*Namson and Davis*, 1988, *Fuis et al*., 2012]. To the north, however, the fault is west dipping whereas south of the Big Bend segment the fault is east dipping. A vertical dip plane in the Big Bend area, therefore, may allow for a more permeable pathway from the mantle, and explain the high R/Ra values reported there. Most depictions of the NIFZ also show it to be a nearly vertical fault at depth [*Wright*, 1991*; Romanyuk et al.*, 2007], perhaps enhancing its ability to transfer mantle components.

Helium isotopic studies of large fault zones including the SAFS, the North Anatolia Fault Zone in Turkey, and the Karakoram fault in Turkey show significant helium anomalies occur only within a distance of 1.0 to 1.5 times the crustal thickness of the area (see *Klemperer et al.*, 2013), indicating crustal scale movement of fluid around these fault zones. In the case of the NIFZ anomaly, the fault is ~2.5 crustal thicknesses distance from the main SAF, yet it shows a

large helium anomaly in multiple samples. The maximum value mantle anomaly (R/Ra = 5.3) is larger than any value measured within the current SAFS, except for the Salton Sea area where the San Andreas fault transitions into the Gulf of California (Figure 1). We think that the NIFZ anomaly is a residual of mantle communication from a paleo subduction zone unrelated to the current SAF. If true, a paleo pathway still exists some 30 million years later, in spite of the eastward shift of the plate boundary and long intervening history of deformation.

4.2 Cause of Local Helium Isotopic Variability

Spatial variability of He anomalies has been previously noted, for example along the SAF [*Kennedy et al*., 1997*; and Kulongoski et al*., 2013]. Helium variability is attributed to "release of radiogenic helium during episodic faulting and fracturing on short time scales" [*Torgerson and O'Donnel,* 1991]. Variability is also attributed to the differences in basement rock, groundwater flow paths, or residence time of mantle helium during transport through the crust [see p. 96 of *Kulongoski et al.*, 2013]. In the case of the NIFZ, variability of isotopic ratios is in part due to variation in contribution of crustal ^{4}He. All of the shallow samples have low R/Ra values relative to the deep samples (Table 2). But some of the deep samples (e.g. Sawtelle and Sansinena fields) also have low R/Ra values indicating the variation in R/Ra values cannot be explained simply by sample depth. In addition, considerable variation in R/Ra may be due to lithological variation. For example, in the Long Beach field, Wells SHP 23-25 and D-81 have relatively low Rc/Ra values (0.54 and 0.55 Ra) compared to adjacent wells. These two wells are perforated over 0.3 km in U-Th enriched shale with up to 25 ppm U and 10 ppm Th, based on spectral gamma ray logs. Similarly, the perforations in Well ALA 49A are just above this zone and may explain the somewhat lower value of 1.0 Ra for this sample relative to most others

along the NIFZ trend. U-Th values for the Miocene section in the vicinity of the NIFZ, based on modern spectral gamma ray logs, are typically 2 to 6 ppm. We interpret the relatively low value of $^{3}He/^{4}He$ (R/Ra = 0.54-.55) in these wells to the production of abundant ^{4}He from the U-Th rich shale interval. The U-Th rich unit is either below the perforation interval or absent in other wells of our study.

The Newport Beach offshore sample is relatively shallow in the sedimentary section (approximately 1 km depth). Thus, for this sample we cannot determine if the relatively low R/Ra value is due to the lack of mantle communication (i.e. low permeability in the fault zone) or abundance of ^{4}He production within the sedimentary section between the mantle and the sample point.

Spatial variability of helium isotopic ratios exists in the Long Beach and adjacent Long Beach Airport fields where we have the greatest sample density. Helium isotopic ratios vary from about 1.0 to 4.0 Ra (excluding Well SHP 23-25 discussed above) over a distance of less than a few kilometers. Temporal variation of the helium anomalies, from duplicate samples of Well B-14, in the Long Beach field over an approximate 20 month time interval, indicate similar values between the early sample (R/Ra = 3.06) and the later sample (R/Ra = 3.62), although the helium content drops by about 40% (Table 1and 2).

4.3 Fluids and Gases Associated with the Helium Isotopic Anomaly

Fluids associated with these gases are dilute Na-Cl fluids (TDS = 18,000-28,000 mg/L) that we interpret as seawater modified by water-rock reactions including clay diagenesis. As is typical of many waters associated with Miocene kerogen in southern California, the deep formation waters also have abundant organic acids [*e.g. see Fisher and Boles*, 1990]. These

fluids may also contain unidentified mantle components, including CO_2 (see below). Oxygen isotopic ratios range from $\delta^{18}O_{SMOW}$ = -0.2 to +2.0 ‰ and deuterium δD from -0.8 to -15.6 ‰. All water samples plot on the positive side of the meteoric water line and tend to form trends orthogonal to the line [*Boles et al*., 2011]. Although our database is biased with fluids from the NIFZ, the formation fluids associated with mantle-enriched helium are similar to deep basin formation fluids where there is less mantle enrichment (e.g. Sawtelle field). The LA basin fluids are similar to the deep fluids in the San Joaquin basin but are less evolved from diagenetic reactions due to lower temperature [*Fisher and Boles*, 1990*; Boles et al*., 2011].

4.4 Evidence for Mantle CO_2

CO_2 is thought to be the carrier gas for mantle helium into the crust based on relatively constant $CO_2/^3He$ values of about $2x10^9$ to 10^{10} as measured from areas with mantle dominated fluids [*Marty and Jambon*, 1987*; Marty and Zimmermann*, 1999]. Fluids from continental crust that are corrected for non-mantle CO_2 sources and that have a high ^3He content, also have $CO_2/^3He$ values of about 10^{10} [*Crossey et al*., 2014].

The CO_2 content of the well head gases for which we could obtain analyses vary from 0.2 to 9.5 mole % (Table 2). These gases are largely methane generated during the maturation of the kerogen in the basin. Formation water, which is largely marine water altered by interaction with the rock, is also produced from most wells. The CO_2 content of casing gas in some wells varies over time and thus the values we report here should be interpreted with caution (see Table 2). Thus, the CO_2 concentrations determined from our sample splits are more comparable to the He values than CO_2 concentrations from company gas reports. The calculated ratios of $CO_2/^3He$ range from about 1.2×10^8 to 8.8×10^{11} and the gases with the most mantle-like values (e.g. Rc/Ra

>3.0) generally have $CO_2/^3He$ ratios less than 10^9, lower than predicted for a pure mantle helium sources. The $^3He/^4He$ ratio inversely correlates with $CO_2/^3He$ (Figure 4). *Burnard et al.* [2012] also report an inverse correlation between $^3He/^4He$ and $C/^3He$, but the carbon in this case is mostly methane. High mantle helium values are reported to positively correlate with CO_2 content of ground waters in the Big Bend area [*Kulongoski et al*., 2013], although potential underlying carbonate sources and sinks are not reported for this area. In the vicinity of the NIFZ, potential sources of CO_2 are thermogenic from kerogen (associated with methane production), breakdown of oxygen-bearing organic acids (e.g. methanogenesis), acidization of carbonate (not applicable to our deep sampled wells), and mantle CO_2. A potential sink for the CO_2 in this system is small amounts of distinctive Fe-rich calcite and dolomite cement found in the more deeply buried sandstones. These cements might account for the lower than expected CO_2 values associated with the mantle He. $CO_2/^3He$ ratios greater than 10^9 may result from an increasing thermogenic or methanogenic CO_2 relative to a background level of mantle He. In the following section we use $\delta^{13}C$ of the CO_2 to distinguish potential sources.

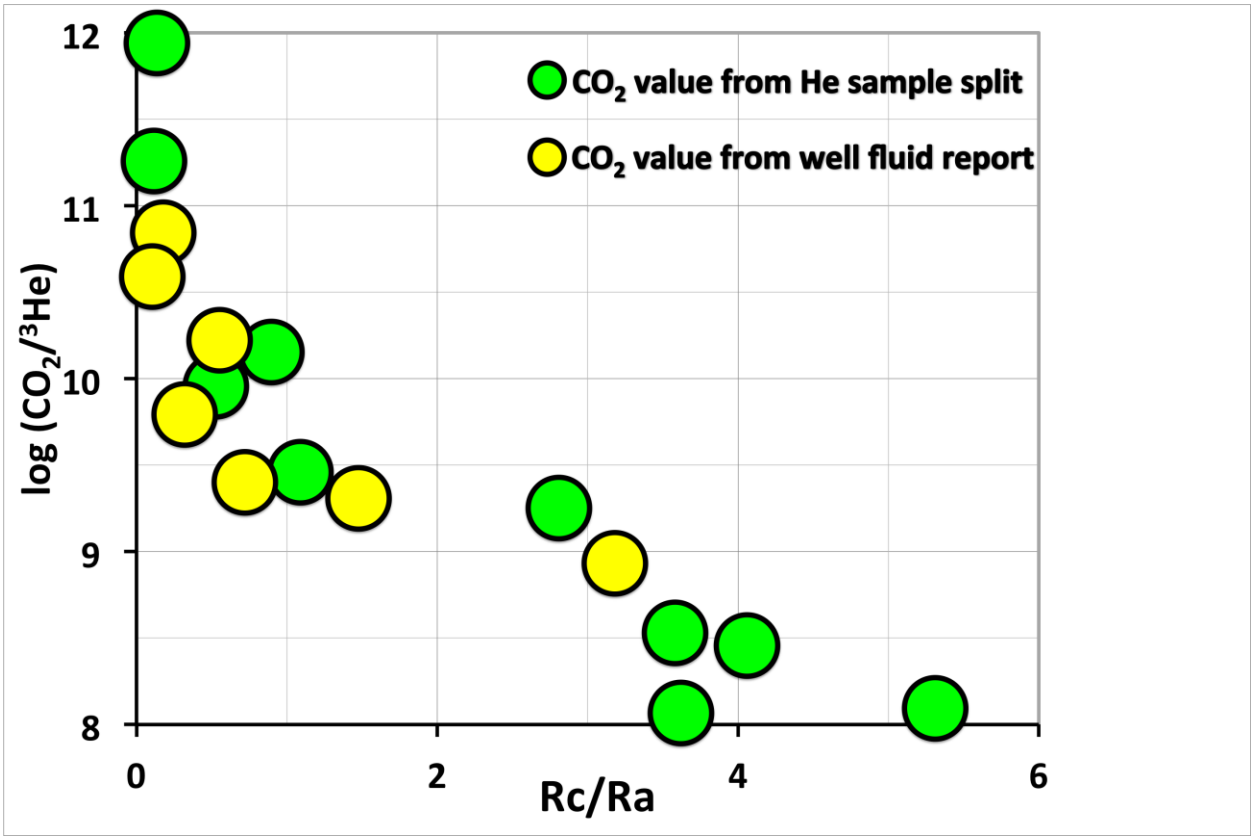

Figure 4. CO_2 / ^{3}He ratio of gas (ppm) plotted against the Rc/Ra value of the gas. CO_2 / ^{3}He ratios of 10^9 to 10^{10} are believed to represent mantle ratios for the carrier gas of CO_2 relative to the mantle-derived ^{3}He in other studies (see text). CO_2 concentration measured from split of ^{3}He sample (green dots). CO_2 concentration from well gas analyses reports (yellow spot). See Table 2 for listing of the data.

MORB CO_2 is reported as having a $\delta^{13}C_{PDB}$ = -6.5+/- 2.5 per mil [*Sano and Marty*, 1995], which is considerably more positive than thermogenic or bacterial CO_2 of $\delta^{13}C_{PDB}$ < -25 to -30 [*Hunt*, 1996], but more negative than CO_2 from methanogenic processes [*Carothers and Kharaka*, 1980]. The $\delta^{13}C_{PDB}$ of carbonate cements in Tertiary sandstones and fault cements of California, which can range from +10 to -40, reflect this wide range of CO_2 sources [*see Boles*, 1998*; Boles et al*., 2004]. As shown below, the $\delta^{13}C$ of CO_2 in the gases of this study indicates a mixture of CO_2 sources.

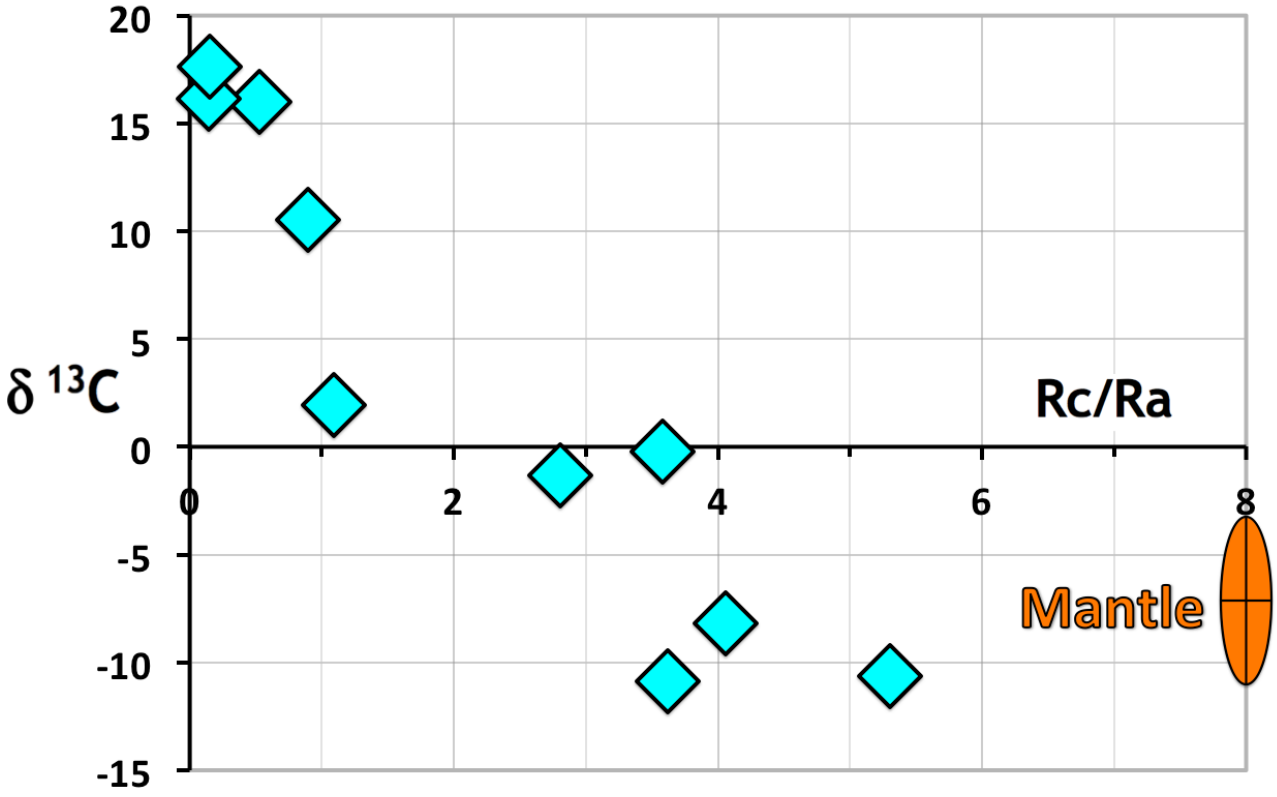

Figure 5. $\delta^{13}C$ ‰ of CO_2 in LA basin gases compared with Rc/Ra of the helium. Note that the low Rc/Ra values are associated with very positive $\delta^{13}C$. Mantle Rc/Ra =8 [Lupton, 1983], mantle $\delta^{13}C$ = 6.5 +/- 2.5‰ [Sano and Marty, 1995]. Data are listed in Table 2.

Figure 5 shows that the Rc/Ra values are inversely correlated with the $\delta^{13}C$ of the CO_2. We interpret this relation as due to mixing between at least two CO_2 sources. At high Rc/Ra values, the CO_2 could be in part mantle derived as the $\delta^{13}C$ values are close to mantle values of $\delta^{13}C$=-6.5+/- 2.5‰. These samples also have the lowest CO_2 content and occur in the deepest reservoirs (Table 1 and 2). None of the samples with high Rc/Ra values appear to have an end member thermogenic CO_2 source. In contrast, the very positive $\delta^{13}C$ values are interpreted to be due to methanogenesis, where the bacterial generation of isotopically light methane leaves a heavy carbon residue. These samples come from relatively shallow reservoirs (<80°C) and have very high CO_2 contents (Table 1 and 2). *Carothers and Kharaka* [1980] have shown very heavy

dissolved carbon ($\delta^{13}C$ up to +28 ‰) in southern California reservoirs at intermediate depths (<80°C) that they attribute to methanogenesis of organic acids. Another source of heavy carbon would be the oxygen bearing functional groups associated with these acids [*Franks et al.*, 2001]. In summary the $\delta^{13}C$ values of the CO_2 indicates mantle CO_2 in the deep LA basin, which is mixed with methanogenic CO_2 in the shallower reservoirs. In the following section, we assume vertical flow and calculate the helium flux along this conduit, and quantify the effect of fluid flow on the thermal structure of the fault zone. We also compute an effective permeability for the NIFZ, based on the helium data signal and estimated fluid pressure gradients for the crust.

5 HELIUM TRANSPORT MODEL

5.1 Theory

We wish to mathematically model the concentrations of the helium isotopes [^3He] and [^4He] along a fluid flow path, as they are transported in the fluid phase, undergo exchange with the country rock, and advected up a fault zone due to a hydraulic gradient. The length of the flow path L is assumed to be approximated by the thickness of the Earth's crust H_c , which is estimated to be about 27-30 km in southern California [*Roymanyuk et al*., 2007]. The isotope ^3He is assumed to derived from magmatic fluids in the Earth's mantle, which may leak up along deep crustal fault zones with sufficient permeability [*Kennedy et al*., 1997]. The isotope ^4He is mostly produced by radioactive decay reactions within various crustal minerals. The goal of this exercise is to mathematically model the helium isotope ratio in the fluid R_f, which will decrease (exponentially) as a mantle-derived fluid moves vertically up the fault zone and becomes increasingly "diluted" by ^4He generated by radiogenic reactions in the crust. Standard porous-flow theory for chemical solute mass balance with isotopic exchange and radiogenic generation

is covered in numerous textbooks and journal articles, too many to review here. For the helium isotope pair, DePaolo (personal communication, 2015) considers the 1-D mass balance, equating the time rate of change of helium mass accumulation/depletion (per unit volume of porous medium) to the advection of the helium isotopes (at a constant pore fluid velocity *v*) and reactive porous exchange and production. He writes this balance as:

$$\frac{\partial C_{f3}}{\partial t} = -v\frac{\partial C_{f3}}{\partial z} + M[RC_{s3} + P_3] \quad (1a)$$

$$\frac{\partial C_{f4}}{\partial t} = -v\frac{\partial C_{f4}}{\partial z} + M[RC_{s4} + P_4] \quad (1b)$$

where *t* is time, *z* is distance, C_f is the concentration of the helium isotope species (^{3}He or ^{4}He) in the fluid at a given time and position, C_s is the concentration of the isotopes in the reactive solid phase, *v* is the average linear fluid velocity [Freeze and Cherry, 1979], *M* is the mass ratio of solid/fluid, *R* is the solid phase dissolution rate, and *P* is the rate of production or generation. It's common practice to combine (1a) and (1b) by assuming $P_3 / P_4 \sim (C_{s3}/C_{s4})$ and define a new model parameter $P'_{He} = [RC_{s4} + P_4]$. The total helium production term J_{tot} (reactive flux of ^{4}He) can also be expressed as: $J_{tot} = M(P'_{He}) = \frac{(1-\phi)\rho_s}{\phi\rho_f}P'_{He}$, where ϕ is fault porosity, ρ_s is density of crustal rocks (solid phase), and ρ_f is density of the fluid phase. Johnson and DePaolo [1994] provide a full derivation of this theory and mathematics, and present an analytical solution for the special case of steady fluid flow, when *v* ~ constant. In Appendix A we show that their analytical solution to (1) can be rewritten as:

$$v = H_c \frac{\rho_s}{\rho_f} \frac{(1-\phi)}{\phi} \frac{P\prime(^4He)}{[He]_{f,m}} \left[\ln \left\{ \frac{\left(R/R_a\right)_m - \left(R/R_a\right)_c}{\left(R/R_a\right)_f - \left(R/R_a\right)_c} \right\} \right]^{-1} \quad (2)$$

after normalizing the fluid, crustal, and mantle isotopic ratios $R = [^3He]/[^4He]$ by the atmospheric helium ratio R_a and defining the helium concentration in the fluid at the mantle source $C_f = [He]_{f,m}$.

A similar expression, depicting the fluid velocity as a function of the helium ratio $(R/Ra)_f$ was first presented by *Kennedy et al.* [1997]. They used their equation to predict the fluid flow rate in the San Andreas fault zone, but did not present a derivation in their article. A similar equation for the fluid velocity is also presented in *Kennedy and van Soest* [2006], *Burnard et al.* [2012], and *Kulongoski et al.* [2013], but again without any published derivation. Appendix A provides more details on our derivation and a comparison of the equations.

5.2 Fluid Flow Rate Calculation

It follows from equation (2) that the predicted fluid velocity v is inversely proportional to the helium concentration in the source fluid (mantle) and the isotopic disequilibrium, for a given fault geometry and reactive flux of radiogenic helium from the crust. We use (2) to estimate the fault-zone fluid velocity, based on the helium measurements and estimated physical parameters. For example, from Well Dominguez #2 (Table 1), assuming H_c = 27 km, ϕ = 0.03, ρ_s = 2.60 gm/cm^3, ρ_f = 1.026 gm/cm^3, $(R/R_a)_m = 8.00R_a$, $(R/R_a)_f = 5.31\ R_a$, and $(R/R_a)_c = 0.02R_a$,

$$v = (5.3471 \times 10^8) \frac{P\prime(^4He)}{[He]_{f,m}} \quad (3)$$

Our estimate for fault porosity ~ 3% represents a representative value, vertically averaged over the entire depth of the fault zone. *Rice* [1992] argued, based on theoretical grounds and magnetotelluric data, that a porosity of about 0.5% to 3% is necessary in the lower crust due to its low electrical resistivity. *Janssen et al.* [2011] measured an effective nano-porosity of 3% from core samples of the San Andreas fault zone (SAFOD site), and *Morrow et al.* [2014] report values of 1.9% to 7.1% for a suite of SAFOD core samples of sandstone, sheared siltstone, cataclasite, and serpentinized clay gouge at a borehole-depth interval ~3,190-3,310 m. Based on these data, we adopted a value of 3% for the NIFZ porosity as a first approximation. Few data sets exist to constrain porosity in deeper fault zones, but we assume it could physically range from 0.03% to 30% depending on the lithology, effective stress, and amount of clay gouge present.

According to *O'Nions and Ballentine* [1993] and *Ballentine and Burnard* [2002], the ^{4}He production rate from radiogenic decay reactions in the crust can be estimated from the known bulk concentrations (ppm) of uranium [U] and thorium [Th]: $P'(^4He)$= (1.207×10^{-13} [U] + 2.867×10^{-14} [Th]). Based on crustal averages [*O'Nions and Oxburgh,* 1988*; O'Nions and Ballentine,* 1993], and gamma log data from the LA basin, we let [U] ~ 2 ppm and [Th] ~ 6 ppm, and therefore we can estimate a production rate, $P'(^4He) = 4.134 \times 10^{-13}$ cm^3 STP/gm-yr. David Graham (Oregon State Univ.-COAS Noble Gas Geochemistry Laboratory, pers. comm. 2015) provides an independent estimate of the "starting" mantle [^{4}He] concentration, as follows: the ocean crust production is about 21 km^3 per year, and the Earth's mantle ^{3}He flux is 1000 moles/yr [*Porcelli and Elliott,* 2008]. If we assume that the Earth's crust is produced by 10% partial melting, and ^{3}He is perfectly incompatible, this gives a mantle [^{3}He] of 3.2×10^{-11} cm^3 STP/g (8.7×10^8 atoms/g). For mantle sources ^{3}He/^{4}He = 8 Ra, this gives [^{4}He] = 3.0×10^{-6} cm^3

STP/g. Relatively gas rich mid-oceanic ridge basalts (MORBs) are reported to have [^{3}He] ~30 cm^3 STP/g, and so if they are derived by 10% partial melting, the value given above is internally consistent with what is observed in MORBs. After substituting $[He]_{f,m} \sim 3.0 \times 10^{-6}$ cm^3 STP/g into (3), we get an average fluid velocity in the fault,

$$v = \frac{2.2105E-04}{[He]_{f,m}} = 73.7\ cm/y \quad (4)$$

or, as the Darcian flow rate (fluid volume discharge rate per unit area), $q = \phi v$ = 2.2 cm/yr. Similar calculations were done for all of our helium gas sample locations in the LA basin (Figure 2), indicating a wide range of predicted flow rates from a low of 0.2 cm/yr (Wilmington and Newport Beach fields) to a high of 2.2 cm/yr (Well Dominguez #2), with flow rate increasing with increasing $(R/Ra)_f$ value and decreasing fault porosity (Figure 6A). The effects of variable fault porosity seem minor, given the likely range expected in the shallow and deep crust.

Based on equation (2), the fluid flow rate scales linearly with the rate of ^{4}He production in the crust (controlled by the U-Th concentrations), and so we have included results (Figure 6B) from a sensitivity study for variable [U] levels, assuming constant U/Th=3. At constant flow rate the U-Th concentration has a marked effect on the R/Ra value, consistent with what we observe in the Long Beach field. The fluid velocity (and flow rate) also increase linearly with the flow path length (~ *Hc*). We have assumed the thickness of the crust as the characteristic length for this model parameter, although one might visualize somewhat longer flow paths, perhaps only by a factor of ~ (1.5-2.0)×H_c (see Figure 7) if helium was being transported along interconnected vertical and lateral fault splays.

For the petroleum reservoir sites with the highest values of $(R/Ra)_f$ > 2, the flow rate trend suggests that the Darcy velocity q ~ 0.2 to 2.2 cm/yr for the LA basin faults. This is twice as fast as the flow rate q ~ 0.1 to 1.0 cm/yr range estimated by *Kennedy et al.* [1997] for the San Andreas fault zone (SAFZ) near Parkfield, California (about 400 km northwest of Long Beach), but slower than the flow rate q ~15 cm/yr recently estimated by *Kulongoski et al.* [2013] for the Big Bend section of the SAFZ in the Cuyama Valley area (about 250 km northwest of Long Beach), all based on helium isotope data.

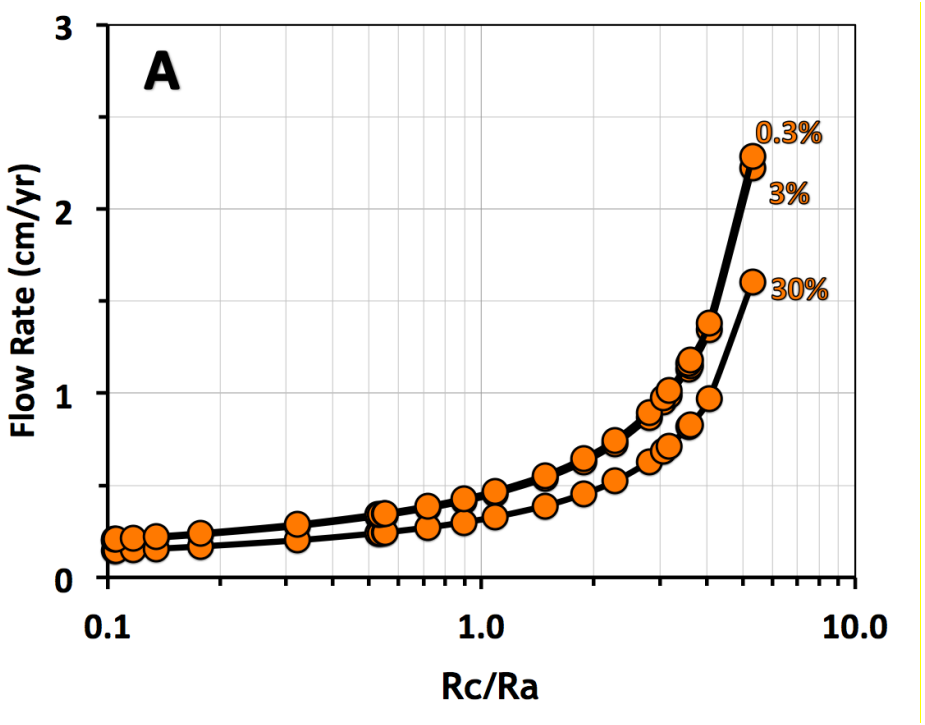

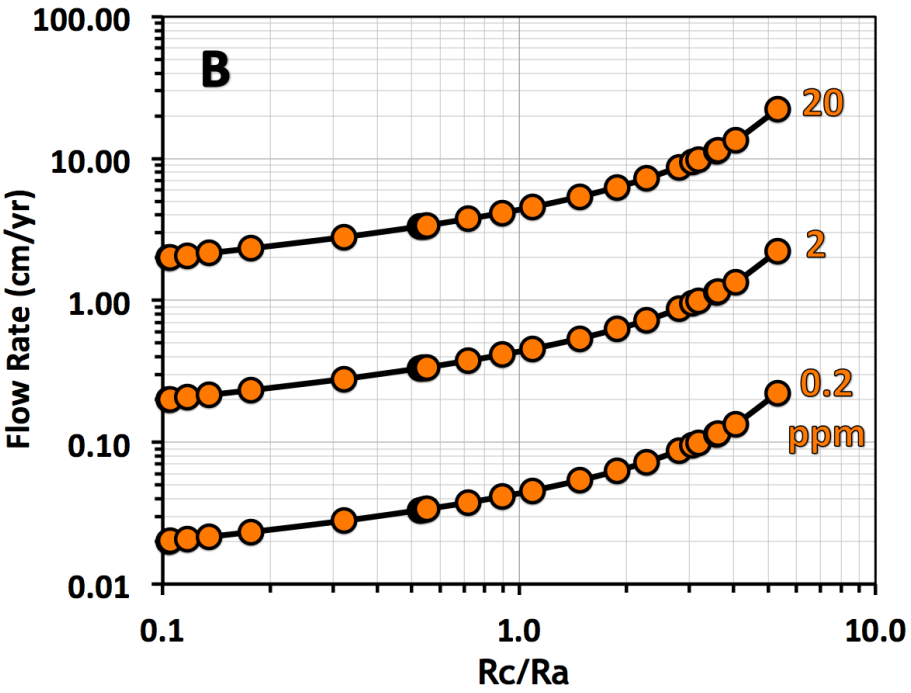

Figure 6. Fluid flow rate (cm/yr) versus air-corrected helium $^{3}He/^{4}He$ ratio, as predicted by a one-dimensional isotopic transport model and well field observations from the LA Basin. Figure 6A shows the effect of fault porosity over a range from 0.3% to 30%. Figure 6B shows the effect of radiogenic flux of ^{4}He, as controlled by the crustal uranium concentration over a range of [U] from 0.2 ppm to 20 ppm. We assume the concentration ratio of [3He/4He]=3 in all three scenarios.

5.3 Thermal Effects of Flow

Given an upper estimate of flow rate $q \sim 2$ cm/yr, we compute a dimensionless "thermal Péclet Number" for the fault-zone flow system, *Pe*, which expresses the ratio of convective heat transport by the fluid flow to bulk conductive heat transfer in the crustal rock [*Betcher,* 1977*; van der Kamp,* 1984*; van der Kamp and Bachu*, 1989*; Person and Garven,* 1992]. For any crustal profile where $Pe > 2$, convective heat flow exceeds conduction, and as a result, anomalous geothermal gradients develop and hot springs would appear in areas of groundwater/fluid discharge [*Anderson, 2005*]. Using the approach and notation of *van der Kamp* [1984], the ratio of convective to conductive heat flow in a basin with 3-D dimensions length *L*, width *W*, and mean height/depth *H*, can be simply represented as:

$$Pe = \frac{\rho_f c_{vf} Q'_f}{\lambda_e \left(L/H\right)} = \frac{Q'_f}{D_e \left(L/H\right)} \quad (5)$$

where ρ_f fluid density, c_{vf} specfic heat capacity of the fluid (at constant volume), Q'_f volumetric fluid flow rate per unit width, λ_e bulk effective thermal conductivity, and D_e bulk thermal diffusion coefficient. We assign the representative fluid and rock parameters [*Ge*, 1998; *Anderson*, 2005]: ρ_f = 1026 kg/m^3, c_{vf} = 4080 J/kg ^{o}C, λ_e = 3.0 W/m °C, and D_e = 7.17 × 10^{-7} m^2/s ~ 23 m^2/yr. Given the local crustal geometry of the LA basin, L ~ 60 km, H ~ 30 km, then (5) simply yields $Pe \sim Q'_f$ /45. For our system, the total volumetric flow rate per unit width of the basin can be expressed as:

$$Q'_f = \frac{qA}{W} = \frac{q\,W\,b_f}{W} = q\,b_f \quad (6)$$

The new parameter b_f = fault zone width. It follows from (5) and (6) that the Péclet Number for the basin domain can be expressed as a function of the Darcy flow rate and fault zone width, and given a representative Darcy flow rate q ~ 0.02 m/yr from the helium data, and assuming a fault width $b_f \sim 150\ m$, we estimate thermal $Pe \sim qb_f/45$ = 0.067 ~ 0.1 for the NIFZ.

Because the disturbance of any conductive subsurface temperature field is due to forced convection (advection) of heat by the fluid phase, the thermal Péclet Number provides a good measure of the degree of thermal disturbance by a fluid flow regime [*van der Kamp and Bachu,* 1989]. It's clear from this dimensional analysis that a vertical flow rate of 2 cm/yr would not perturb the conductive temperature field, but flow rates above 30 cm/yr or higher might. Heat flow measured using idle petroleum wells along the NIFZ indicates a remarkably uniform heat flux of 63 to 66 mW/m^2 [*Price et al*., 1999*; Williams et al*., 2001], extending over 40 km from Seal Beach in the southeast to Inglewood in the northwest. Our low Péclet Number calculation

confirms that the fluid flow rates in the fault zone, as estimated by the helium data, would be too low to perturb the nearly uniform conductive field in this section of the LA basin.

5.4 Fault Permeability Calculation

For a fractured medium, the fluid flow rate per unit area (specific discharge) q can be formally expressed by a one-dimensional form of Darcy's Law, written out in terms of fluid pressure P and elevation Z above a datum [*Hubbert*, 1940]:

$$q = -\frac{k}{\mu_f}\left\{\frac{\partial P}{\partial Z} + \rho_f g\right\} \quad (7)$$

where g is gravitational acceleration, μ_f dynamic viscosity of the fluid, and k the intrinsic permeability (fault zone permeability). This formulation of Darcy's Law assumes a liquid phase fluid of uniform composition. Pre-petroleum industry development of reservoirs in the LA basin indicate a slightly over-pressured sedimentary basin [*Berry*,1973*; Glassley*,2015]. Pore pressures in the lower crust below the basin are unknown, but given this tectonic system is transpressional, one would expect pressure gradients well above hydrostatic of (~0.45 psi/ft), but below geostatic (~1.20 psi/ft), based on the geomechanical reasoning of *Rice* [1992] and *Neuzil* [1995, 2003], and the metamorphic geochemistry and thermal reasoning of *Manning and Ingebritsen* [*1999*]. Therefore, as a first approximation we assume dP/dZ ~ - 0.7 psi/ft (-15,835 Pa/m), as a representative gradient over the thickness of crust. If we assign a Darcy velocity from the Well Dominguez #2, q = 2.2 cm/yr = 0.909 × 10^{-9} m/s, specific weight ρ_f g = 10,055 N/m^3 , and dynamic viscosity μ_f = 0.001 Pa s, then Darcy's Law (7) yields an estimate of the intrinsic permeability:

$$k = -\frac{q\mu_f}{\left\{\frac{\partial P}{\partial Z} + \rho_f g\right\}} \sim 1.58 \times 10^{-16}\, m^2 \qquad (8)$$

or k ~ 158 microdarcys for the NIFZ at this site, vertically averaged over the thickness of the crust. We performed similar calculations for the other gas sample sites, which produces a root-mean-square average permeability k ~ 57 microdarcys (= 5.63×10^{-17} m^2 or log k~ -16.25). For comparison, *Bredehoeft and Ingebritsen* [1990] assigned values of porosity (1%) and compressibility (10^{-4} MPa^{-1}) to estimate a bulk crust permeability of k ~10^{-21} m^2, needed to maintain high fluid pressures thought to exist in the ductile parts of the deep crust. *Morrow et al.* [2014] measured cm-scale lab permeabilities k ~ 10^{-22} to 10^{-18} m^2 on core samples (depth ~2.7 km) of clay-rich gouge from the San Andreas fault at Parkfield, CA. *Rice* [1992], however, argued on theoretical grounds for a km-scale permeability k ~10^{-18} m^2 (1 microdarcy) at the base of the seismogenic zone (depth~15-20 km), by taking into account the depth dependency of bulk rock compressibility on stress. Our helium-based estimate for the NIFZ permeability range, -16.7 < log k < -15.7 m^2, is higher than the exponential depth-dependent range (-18.5 < log k < -16.6 m^2) cited by *Manning and Ingebritsen* [1999], as constrained by thermal data for the Coast Ranges, California, for depths < 15 km. But more recently, *Ingebritsen and Manning* [2010] have proposed log k > -16 m^2 for high-permeability transients (t ~ 10^3 years), particularly for fault and shear zones in the brittle crust (depths < 10 km), and an upper limit (constant) log k ~ -16 m^2 for the ductile crust (depths > 15 km). Giger et al. [2007] used hot-press high P-T experiments to show that, within the recurrence time interval of large earthquakes, quartz-rich fault zones in the middle to lower crust can evolve from high-permeability conduits to low-permeability seals. Under lower crustal temperatures of 600-800 ^oC, permeability typically exceeds ~ 10^{-19} m^2 , and follows the well-known cubic law $k \sim \phi^3$, provided fault gouge porosity exceeds ~ 4%.

6 DISCUSSION

Mantle seepage into the NIFZ has important implications with respect to structural models for the deep LA basin. Specifically, recent models using kinematic balanced cross-sections propose that the NIFZ is cut off and offset from the deeper crust by a deep (8-10 km) sub-horizontal thrust ramp that is part of a central basin décollement [see Figure 7; *Davis et al.*, 1989*; Shaw and Suppe,* 1996]. However, our geochemical data indicate that the NIFZ is the only major fault in the basin that is connected to the very deep crust. If the structural interpretation of *Shaw and Suppe* [1996] is correct, the blind thrust, presumably a shortening feature, is a pathway for at least four km of lateral transport of helium. Alternatively, the model may be incorrect and the NIFZ may extend directly to the mantle unaffected by the proposed underlying faults.

Several lines of evidence, not necessarily consistent with each other, indicate the NIFZ is an area with some anomalous deep crustal features. These features may relate to the paleo-subduction zone (plate boundary) proposed by *Hill* [1971]. Analysis of teleseismic events in the Long Beach area from a 3D seismic array at Signal Hill indicates the Moho may have 10 km of vertical offset approximately 10 km to the south of the NIFZ in the Long Beach area [*Schmandt and Clayton,* 2013]. The model projects a 65° north-dipping surface to the offset, which would project about 30 km south of the NIFZ (Figure 7). The offset of the Moho at this locality may connect to thrusting along the Palos Verdes fault (see Figure 2) and if so, then the mantle communication between the Moho and the surface is weaker here than along the NIFZ, based on the strength of the R/Ra ratio in the two areas (Figure 2). Another study, based on gravity and seismic data, concludes the NIFZ is the southwest boundary between a thick section of ultramafic lower crust on the north and a thin section of oceanic crust to the south [see Figure 8

of *Romanyuk et al.*, 2007]. The abrupt lateral change in lithospheric material in the deep crust adjacent to the NIFZ is consistent with a deep-seated conduit to the Moho along the NIFZ and the preservation of a paleo-subduction boundary.

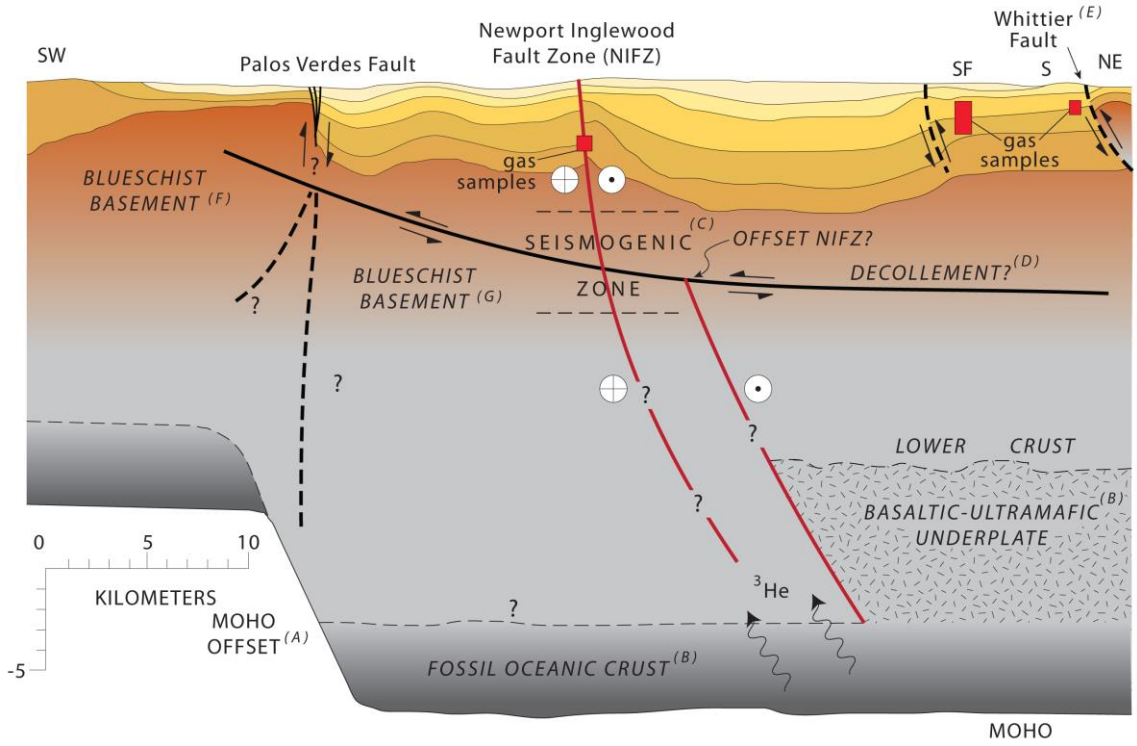

Figure 7. Geologic cross section of the Los Angeles basin, from the southwest to northeast. This profile intersects the NIFZ at Long Beach (see section line on Figure 2). The cross section is shown without vertical exaggeration. Deep basin features include: the offset Moho (A), the basaltic-ultramafic under plating adjacent to the NIFZ (B), seismogenic zone along the NIFZ (C), the proposed décollement underlying the LA basin, including the offset of the NIFZ along the décollement (D), the northern basin Whittier fault (E), and the blueschist basement southwest of the NIFZ (F). See text for references and discussion of basin features. The helium isotopic data indicate that the NIFZ is a permeable connection to the mantle for this part of the crust.

7 CONCLUSIONS

Leakage of mantle helium into the lower crust without associated elevated heat may be explained by ~ 0.2 to 2.0 cm/yr fluid flux rates, sufficiently high enough to transport ^{3}He from

the mantle, but at rates too slow to disturb conductive heat transfer. Transport of ^{3}He without dilution by ^{4}He from the crust requires relatively rapid movement of mantle gas along preferred pathways without long residence time. This also implies local transport of heat. Our calculations suggest flux rates of up to about 2 cm/year, which would be insufficient to perturb the ambient conductive heat flow, due to the low thermal Peclet Number. Our geochemical modeling of helium transport also suggests a time-averaged fault permeability $k \sim 5.6 \times 10^{-17}$ m^2 (60 microdarcys) for the NIFZ, which compares well with estimates for deep crustal fluid flow from other geophysical data sets.

Sampling for mantle helium anomalies generally focuses on areas with thermal anomalies [*Oxburgh et al.,* 1986*; Hilton et al.,* 2002*; Kennedy and van Soest,* 2007*; Umeda et al.,* 2007]. The flux of mantle helium into the continental crust needs to be re-evaluated by more extensive gas sampling in faulted areas with normal geothermal gradients. In addition, the importance of understanding local geology is demonstrated by the effects of elevated U-Th concentration on observed R/Ra values.

Our findings suggest that the NIFZ is a likely fluid conduit through the seismogenic zone and lower crust to the upper mantle. Although we cannot be certain that the NIFZ is not connected to other mantle-connected faults at depth, we believe the NIFZ itself, based on the evidence discussed above, including strength and consistency of the signal and geologic setting, is the likely primary pathway of mantle fluids in the area. This suggests the fault continues to be a fundamental boundary in the LA basin.

The mantle connection along the NIFZ has apparently persisted since early Miocene time in spite of the eastward migration (80 km jump?) of the plate boundary and the proposed,

potentially seismically active décollement within the deep LA basin. It appears to be an example of relatively "slow" seepage of mantle fluids from a paleo-subduction zone.

ACKNOWLEDGMENTS

This research was supported by the U.S. Department of Energy (Office of Science, and Office of Basic Energy Sciences) under award numbers DE-SC-0003676 (Boles) and DE-FG02-07ER15900 (Garven), and by the NOAA Pacific Marine Environmental Laboratory (Lupton). We are grateful to the following organizations for permission to sample: Signal Hill Petroleum, Inc.; Occidental Oil & Gas Corp (California Resources Corp), Breitburn Energy Partners, LP; City of Newport Beach; Decor LLC; and Freeport-McMoRan, Inc. The paper benefitted by comments from Brady Barto (Signal Hill Petroleum), Peter Eichhubl (Bureau of Economic Geology, University of Texas-Austin), and editing by Stacey Zeck-Boles. Thom Davis provided insight into the structural aspects of southern California faults. The second author is very grateful for helpful discussions about isotopes with his sabbatical faculty host Jennifer McIntosh (University of Arizona), and Tufts faculty colleagues Anne Gardulski (Earth and Ocean Sciences), James Adler (Department of Mathematics) and Andrew Ramsburg (Department of Civil and Environmental Engineering), and for the helium-distance regression analysis by Tufts alumnus Ellen Garven (Department of Physics). Don DePaolo (LBNL) and Tom Johnson (UIUC) provided useful guidance on isotope modeling, and Ghislain de Marsily (professeur émérite, Université Pierre et Marie Curie) and Philippe Ackerer (CNRS, France, Lab. d'Hydrologie et de Géochimie de Strasbourg) provided very useful information on the behavior of tracers in large groundwater systems. We thank Leigh Evans for helium isotope analysis. The CO_2 concentrations and isotopic values were determined by Marvin Lilley, who thanks Stefano

Bernasconi and Gretchen Früh-Green for access to the instrumentation in the Geological Institute at the ETH Zürich. This is PMEL publication number 4339. We note that there are no data sharing issues since all of the numerical information is provided in figures and tables in the paper.

APPENDIX A

Derivation of the Helium Flow Rate Equation

Based on the theory and notation of *Johnson and DePaolo* [1994, 1997], the mass concentration ratio of an isotope pair (e.g. [^{3}He]/[^{4}He]) can be represented mathematically by combining the aqueous mass conservation equations for each isotope into a single partial differential equation, and casting the isotopic ratio in the fluid phase R_f as the sole dependent variable:

$$\frac{\partial R_f}{\partial t'} = \frac{1}{P_e}\left(\frac{\partial^2 R_f}{\partial z'^2} + \frac{2}{c_f}\frac{\partial c_f}{\partial z'}\frac{\partial R_f}{\partial z'}\right) - \frac{\partial R_f}{\partial z'} + D_a[\bar{R}_d - R_f] \qquad \text{(A-1)}$$

This equation describes mass conservation (per unit volume of bulk porous medium) of the helium isotope ratio, $R = [^3He]/[^4He]$, assuming a one-dimensional transport field (z distance along the flow path) where isotopic mass is advected by the flow field and undergoes diffusion (mixing) and isotopic exchange. We define the following variables and parameters in (A-1): $z' = z/L$ dimensionless distance, L = length of the domain, $t' = \{(tv)/L\}$ dimensionless time, v average pore-fluid velocity, R_f isotope ratio in the moving fluid phase, R_d isotope ratio of the radiogenic decay flux from the solid phase, c_f source concentration of the isotope in the fluid

phase (mass/fluid volume), $P_e = \{(vL) / D\}$ chemical Péclet Number (ratio of advective mass flux /diffusive mass flux), $D_a = \{ (L\ J_{tot}) / (v\ c_f) \}$ Damköhler Number (ratio of reactive mass flux/advective mass flux), and J_{tot} total reactive flux (total mass of the radiogenic isotope delivered to a unit volume of fluid by all reactions per unit time). Generally speaking, in fault zones Pe >> 1, and advection greatly dominates over processes of diffusion [*Phillips*, 1991].

The full derivation of equation (A-1) is given by *Johnson and DePaolo* [1994] and they assume: i) one-dimensional mass transport by advection and diffusion, ii) uniform and steady rate of advection of the isotopic species under a constant pore-fluid velocity v in the fault zone, iii) homogeneous and constant porosity, iv) homogeneous fluid density and viscosity, and v) uniform and constant reaction flux J_{tot} due to radiogenic production of ^{4}He. If we adopt the additional mathematical simplifications of *Johnson and DePaolo* [1994] and consider the special case of steady-state mass transport (i.e. $\partial R_f / \partial t' \sim 0$), and assume negligible effects of diffusion of the isotopic mass (i.e. $D \sim 0$), then (A-1) simplifies to:

$$\frac{dR_f}{dz'} = -D_a[R_f - \bar{R}_c] \qquad \text{(A-2)}$$

where we have set $\bar{R}_d = \bar{R}_c$, the average "crustal" ratio, and assume this is nearly constant.
To solve for the unknown dependent variable R_f, *Johnson and DePaolo* [1994] integrate (A-2) over the isotope ratio range on the boundaries for 1-D transport,

$$\int_{r_{f,o}}^{r_f} \frac{1}{[R_f - \bar{R}_c]}\, dR_f = ln\left\{\frac{[R_f - \bar{R}_c]}{[R_{f,o} - \bar{R}_c]}\right\} = -D_a[z'] \qquad \text{(A-3)}$$

With re-arranging terms in (A-3) to simplify, as done by *Johnson and DePaolo* [1994], their equation (23), p. 1575], we get:

$$R_f(z') = \bar{R}_c + [R_{f,0} - \bar{R}_c] \exp\{-D_a z'\} \quad \text{(A-4)}$$

For the outflow boundary, where z'=1 (i.e. $z = L = H_c$), it follows from (A-4) that

$$\frac{[R_f - \bar{R}_c]}{[R_{f,0} - \bar{R}_c]} = \frac{(R_f - \bar{R}_c)}{(R_m - \bar{R}_c)} = \exp\{-D_a\} = \exp\{-\frac{H_c J_{tot}}{v\, c_f}\} \quad \text{(A-5)}$$

where $R_{f,o} = R_m$ is the helium isotope ratio of the fluid at the inflow boundary z'=0 (i.e. mantle/crust inflow boundary). Based on the closed-form solution (A-5), the isotopic disequilibrium term $[\bar{R}_c - R_f]$ will decay exponentially with distance traveled, with the Damköhler Number D_a as the exponential factor (assumed constant), as correctly noted by *Johnson and DePaolo* [1994]. Solving (A-5) for the average linear fluid velocity v [see *Bear*, 1972; *Freeze and Cherry*, 1979] in the fault zone yields,

$$v = -\frac{H_c J_{tot}}{c_f \ln\left\{\frac{(R_f - \bar{R}_c)}{(R_m - \bar{R}_c)}\right\}} \quad \text{(A-6)}$$

After bringing the minus sign into the logarithmic term and rearranging this equation,

$$v = \frac{H_c J_{tot}}{c_f \ln\left\{\frac{(R_m - \bar{R}_c)}{(R_f - \bar{R}_c)}\right\}} = \frac{H_c J_{tot}}{c_f}\left[\ln\left\{\frac{(R_m - \bar{R}_c)}{(R_f - \bar{R}_c)}\right\}\right]^{-1} \quad \text{(A-7)}$$

It's clear from this equation that the predicted fluid velocity v is inversely proportional to the helium concentration in the source fluid (mantle) and the isotopic disequilibrium, for a given fault geometry and reactive flux of radiogenic helium from the crust. Based on the notation in

Johnson and DePaolo [1994] and *Kennedy et al.* [1997], the total helium production term J_{tot} (reactive flux of ^{4}He) can be expressed as:

$$J_{tot} = M(P'_{He}) = \frac{(1-\phi)\rho_s}{\phi\rho_f} P'_{He} \quad \text{(A-8)}$$

where M is the mass ratio of solid to fluid phases (per unit bulk volume), P'_{He}= radiogenic helium production rate from the crust (~ constant) , ϕ = fault porosity, ρ_s = density of crustal rocks (solid phase), and ρ_f = density of fracture-zone fluid (fluid phase). Inserting this expression for J_{tot} into (A-7), and redefining the parameter constant $c_f = [\mathrm{He}]_{f,m}$, to be consistent with *Kennedy et al.* [1997] notation, equation (A-8) now can be reformatted, after normalizing the fluid, crustal, and mantle isotopic ratios by the atmospheric helium ratio R_a, such that:

$$v = H_c \frac{\rho_s}{\rho_f} \frac{(1-\phi)}{\phi} \frac{P\prime(^4He)}{[He]_{f,m}} \left[\ln \left\{ \frac{\left(R/R_a\right)_m - \left(R/R_a\right)_c}{\left(R/R_a\right)_f - \left(R/R_a\right)_c} \right\} \right]^{-1} \quad \text{(A-9)}$$

Equations (A-7) and (A-9) are similar to the working equation first presented in *Kennedy* et al. [1997], but they appear to have simplified it further by assuming (1 - ϕ) ~ 1 for very small porosity, and they appear to have replaced the logarithm term with the Taylor Series approximation ln{x} ~ (1- x), which is mathematically valid for estimates of the argument x ~ 1. To verify their derivation and compare to ours, consider a Taylor Series expansion of a logarithmic function (centered at 1, for 0<x<2): $\ln(x) = \frac{(x-1)^1}{1} - \frac{(x-1)^2}{2} + \frac{(x-1)^3}{3} - + \ldots$ If the argument $x \sim 1$, then $ln\ (x) \sim (x-1)$ is the first-order Taylor approximation. Therefore, equation (A-7) could be rewritten,

$$v = \frac{H_c J_{tot}}{c_f\left(\frac{r_m - \bar{r}_c}{r_f - \bar{r}_c} - 1\right)} = \frac{H_c J_{tot}}{c_f\left(\frac{r_m - \bar{r}_c - r_f + \bar{r}_c}{r_f - \bar{r}_c}\right)} = \frac{H_c J_{tot}}{c_f\left(\frac{r_m - r_f}{r_f - \bar{r}_c}\right)} = \frac{H_c J_{tot}}{c_f}\left(\frac{r_f - \bar{r}_c}{r_m - r_f}\right) \quad \text{(A-10)}$$

Furthermore, based on the notation in *Johnson and DePaolo* [1994], the total helium production term J_{tot} (reactive flux of ^{4}He due to radiogenic reactions) can be expressed as:

$$J_{tot} = M(P'_{He}) = \frac{(1-\phi)\rho_s}{\phi\rho_f} P'_{He} \sim \frac{\rho_s}{\phi\rho_f} P'_{He} \quad \text{(A-11)}$$

which assumes $(1-\phi) \sim 1.0$, or in other words that porosity ϕ is very small. Inserting this expression for J_{tot} into (A-10), and redefining $c_f = [\mathrm{He}]_{f,m}$ as before, we get:

$$v = \frac{H_c \frac{\rho_s}{\phi\rho_f} P'_{He}}{c_f}\left(\frac{R_f - \bar{R}_c}{R_m - R_f}\right) = \frac{H_c \rho_s P'_{He}}{\phi\rho_f [\mathrm{He}]_{f,m}}\left(\frac{R_f - \bar{R}_c}{R_m - R_f}\right) \quad \text{(A-12)}$$

The Darcy velocity q, also known as the specific discharge (volumetric flow rate per unit area of porous medium) is defined by Forchheimer's formula [*Bear*, 1972], $q = v\phi$, and therefore we can rewrite (A-12) as:

$$q = \frac{H_c \rho_s P'_{He}}{\rho_f [\mathrm{He}]_{f,m}}\left(\frac{R_f - \bar{R}_c}{R_m - R_f}\right) \quad \text{(A-13)}$$

This is the simplified equation format first presented by *Kennedy et al.* [1997]. We decided to use equation (A-9) for our calculations of flow rates, because application of the Kennedy equation (A-13) generated computational errors of up to 50% for the NIFZ physiochemical parameters.

REFERENCES

Anderson, M.P. (2005), Heat as a ground water tracer, *Groundwater*, **43**, doi:10.1111/j.1745-6584.2005.00052.x.

Andrews, J.N. (1985), The isotopic composition of radiogenic He and its use to study ground water movement in confined aquifers, *Chemical Geology*, **49**, 339-351.

Ballentine, C.J. and P.G. Burnard (2002), Production and release of noble gases in the continental crust, *Rev. Mineralogy and Geochemistry*, **47**, 481-538.

Bear, J. (1972), *Dynamics of Fluids in Porous Media*, American Elsevier, New York, 764 p.

Berry, F.A.F. (1973), High fluid potentials in California Coast Ranges and their tectonic significance, *AAPG Bulletin*, **57**, 1219–1249.

Betcher, R.N. (1977), *Temperature Distributions in Deep Groundwater Flow Systems – A Finite Element Model*, MS Thesis, University of Waterloo, Canada.

Bredehoeft, J.D., and S.E. Ingebritsen (1990), Degassing of carbon dioxide as a possible source of high pore pressures in the crust. In: *The Role of Fluids in Crustal Processes*, edited by Bredehoeft, J.D. and D.L. Norton , National Academy Press, Washington, D.C., 158–164.

Bjorklund, T. (2003), The Whittier fault trend: Cross sections, structure maps and well tops in the major oil producing area of the northeastern Los Angeles basin, *AAPG Search and Discovery Article* #10038.

Boles, J.R. (1998), Carbonate cementation in Tertiary sandstones, San Joaquin basin, California, *Spec. Pub. Internat. Assoc. Sediment*., **26**, 261-283.

Boles, J. R., P. Eichubl, G. Garven, and J. Chen (2004), Evolution of a hydrocarbon migration pathway along a basin bounding fault: Evidence from fault cements, *AAPG Bulletin*, **88**, 947-970.

Boles, J.R, G. Garven, M. Mallory, and M. Camacho (2011), Differences in formation water composition in arkosic California basins: Implications for types of water-rock interaction and fluid transfer, *Abstract H13A-1187 presented at 2011 Fall Meeting, AGU*, San Francisco, Calif., 5-9 Dec.

Burnard, P., S. Bourlange, P. Henry, L. Geli, M.D. Tryon, B. Natal'in, A.M.C. Sengör, M.S. Özeren and M.N. Çagatay (2012), Constraints on fluid origins and migration velocities along the Marmara main fault (Sea of Marmara, Turkey) using helium isotopes, *Earth Plant. Sci. Letters* **341-344**, 68-78.

Carothers, W.W. and Y.K. Kharaka (1980), Stable carbon isotopes of HCO_3^- in oil-field waters—implications for the origin of CO_2, *Geochimica et Cosmochimica Acta*, **44**, 323-332.

Crossey, L.J., K.E. Karlsom, A.E.Springer, D. Newell, D.R.Hilton, and T. Fischer (2014) Degassing of mantle-derived CO2 and He from springs in the southern Colorado Plateau –

Neotectonics connections and implications for groundwater systems, *GSA Bulletin*, **121**, 1034-1153.

Davis, T.L., J. Namson, and R.F. Yerkes (1989), A cross section of the Los Angeles area: seismically active fold and thrust belt, the 1987 Whittier narrows earthquake and earthquake hazard, *Journal of Geophysical Research*, **94**, 9644-9664.

DePaolo, D.J. (2006), Isotopic effects in fracture-dominated reactive fluid-rock systems, *Geochimica et Cosmochimica Acta*, **70**, 1077-1096, doi:10.1016/j.gca.2005.11.022.

Du, J., W. Cheng, Y. Zhang, C. Jie, Z. Guan, W. Liu, and L. Bai (2006), Helium and carbon isotopic composition of thermal springs in the earthquake zone of Sichuan, southwestern China: *Jour. Asian Earth Sci*., **26**, 533-539.

Fisher, J.B., and J.R. Boles (1990), Water-rock interaction in Tertiary sandstones in the San Joaquin basin, California, USA, *Chemical Geology*, **82**, 83-101.

Franks, S.G., R.F. Dias, K.H. Freeman, J.R. Boles, A. Holba, A.L. Fincannon, and E.D. Jordan (2001), Carbon isotopic composition of organic acids in oil field waters, San Joaquin Basin, California, USA, *Geochimica et Cosmochimica Acta*, **65** (8), 1301-1310.

Freeze, R.A. and J.A. Cherry (1979), *Groundwater*, Prentice-Hall, Englewood Cliffs, NJ, 604 p.

Fuis, G.S., D. S. Scheirer, V. E. Langenheim, and M. D. Kohler (2012), A new perspective on the geometry of the San Andreas Fault in Southern California and its relationship to lithospheric structure, *Bulletin of the Seismological Society of America*, **102**(1), 236–251.

Gautheron, C. and M. Moreira (2002), Helium signature of the subcontinental mantle, *Earth Planet. Sci. Letters*, **199**, 39-47.

Ge, S. (1998), Estimation of groundwater velocity in localized fracture zones from well temperature profiles, *J. Volcanology and Geothermal Research*, **84**, 93-101.

Giger, S.B., E. Tenthorey, S.F. Cox, and J.D. Fitz Gerald (2007), Permeability evolution in quartz fault gouges under hydrothermal conditions, *J. Geophys. Res.*, **112**, B07202, doi: 10.1029/2006JB004828.

Glassley, W.E. (2015), *Geothermal Energy, Renewable Energy and the Environment*, 2nd ed., CRC Press, 378 p.

Güleç, N., D.R. Hilton, and H. Mutlu (2002), Helium isotope ratios in Turkey: relationship to tectonics, volcanism, and recent seismic activity, *Chemical Geology*, **187**, 129-142.

Harding,T.P.(1973), Newport-Inglewood trend, California- An example of wrenching style deformation, *AAPG Bulletin*, **57**, 97-116.

Hauksson, E. (1987), Seismotectonics of the Newport-Inglewood fault zone in the Los Angeles basin, southern California, *Bulletin of the Seismological Society of America*, **77**, 539-561.

Hauksson, E. (1990), Earthquakes, faulting, and stress in the Los Angeles basin, *Journal of Geophysical Research*, **95**, 15365-15394.

Heidbach, O., M. Tingay, A. Barth, J. Reinecker, D. Kurfeß, and B. Müller (2008), The World Stress Map database release 2008 doi:10.1594/GFZ.WSM.Rel2008.

Hill, M.L. (1971), Newport-Inglewood zone and Mesozoic subduction, *GSA Bulletin*, **82**, 2957-2962.

Hilton, D.R., T.P. Fisher, and B. Marty (2002), Noble gases and volatile recycling at subduction zones, *Reviews in Mineralogy*, **47**, 319-370.

Hubbert, M.K. (1940), The theory of ground-water motion, *Journal of Geology*, **48**, 785-944.

Hunt, J.M. (1995), *Petroleum Geochemistry and Geology* , 2nd ed., W.H.Freeman, 743p.

Ingebritsen, S.E., and C.E. Manning (2010), Permeability of the continental crust: dynamic variations inferred from seismicity and metamorphism, *Geofluids*, **10**, 193-205, doi: 10.1111/j.1468-8123.2010.00278.x.

Janssen, C., R. Wirth, A. Reinicke, E. Rybacki, R. Naumann, H-R. Wenk, and G. Dresen (2011), Nanoscale porosity in SAFOD core samples (San Andreas Fault), *Earth Planetary Sci. Letters*, **301**, 179-189, doi: 10.1016/j.epsl.2010.10.040.

Jenden, P., I.R. Kaplan, R.J. Poreda, and H. Craig (1988), Origin of nitrogen-rich gases in the California Great valley: Evidence from helium, carbon, and nitrogen isotope ratios, *Geochimica et Cosmochimica Acta*, **52**, 851-861.

Jung, B., G. Garven, and J.R. Boles (2015), The geodynamics of faults and petroleum migration in the Los Angeles Basin, *American Journal of Science*, **315**, 413-460, DOI 10.2475/05.2015.02.

Johnson, T.M. and D.J. DePaolo (1994), Interpretation of isotopic data in groundwater-rock systems: model development and application to Sr isotope data from Yucca Mountain, *Water Resources Research*, **30**, 1571-1587.

Kamensky, I.L., I.N. Tolstik, and V.R. Vetrin, (1990), Juvenile helium in ancient rocks: I. ^{3}He excess in amphiboles from 2.8 Ga charnokite series- crust-mantle fluid in intercrustal magmatic processes, *Geochimica et Cosmochimica Acta*, **54**, 3115-3122.

Kennedy, B.M., Y.K. Kharaka, W.C. Evans, A. Ellwood, D.J. DePaolo, J. Thordsen, G. Ambats, and R.H. Mariner (1997), Mantle fluids in the San Andreas fault system, California, *Science*, **278**, 1278-1281.

Kennedy, B.M, and M.C. van Soest (2006), A helium isotope perspective on the Dixie Valley, Nevada, hydrothermal system, *Geothermics*, **35**, 26-43.

Kennedy, B.M., and M.C. van Soest, M.C. (2007), Flow of mantle fluids through the ductile lower crust, *Science*, **318**, 1433-1436.

Klemperer, S.L., M.K. Kennedy, S.R. Sastry, and Y. Makovsky (2013), Mantle fluids in the Karakoram fault: Helium isotope evidence, *Earth Planetary Sci. Letters*, **366,** 59-70.

Kulongoski, J.T., D.R. Hilton, P.H. Barry, B.K. Esser, D. Hillegonds, and K. Belitz, (2013), Volatile fluxes through the Big Bend section of the San Andreas Fault, California: Helium and carbon-dioxide systematics, *Chemical Geology*, **339**, 92-102.

Lowenstern, J.B., W.C. Evans, D. Bergfeld, and A.G. Hunt (2014), Prodigious degassing of a billion years of accumulated radiogenic helium at Yellowstone, *Nature*, **506**, 355-358.

Lupton, J.E. (1983), Terrestrial inert gases: isotope tracer studies and primordial components in the mantle, *Annual Review of Earth and Planetary Science*, **11**, 371- 414.

Manning, C.E., and S.E. Ingebritsen (1999), Permeability of the continental crust: implications of geothermal data and metamorphic systems, *Reviews of Geophysics*, **37**, 127-150.

Marty, B., and A. Jambon (1987), C/^{3}He in volatile fluxes from the solid Earth: Implications for carbon geodynamics, *Earth Planetary Sci. Letters*, **83**, 16-26.

Marty, B., and L. Zimmermann (1999), Volatiles (He, C, N, Ar) in mid-ocean ridge basalts: assessment of shallow-level fractionation and characterization of source composition, *Geochimica et Cosmochimica Acta*, **63**, 3619-3633.

Morrow, C.A., D.A. Lockner, D.E. Moore, and S. Hickman (2014), Deep permeability of the San Andreas Fault from San Andreas Observatory at Depth (SAFOD) core samples, *Journal of Structural Geology*, **64**, 99-114.
Namson, J. and T. Davis (1988), Structural transect of the western transverse ranges, California: implications for lithospheric kinematics and seismic risk evaluation, *Geology*, **16**, 675-679.

Neuzil, C.E. (1995), Abnormal pressures as hydrodynamic phenomena, *American Journal of Sciences*, **295** (6), 742-786.

Neuzil, C.E. (2003), Hydromechanical coupling in geologic processes, *Hydrogeology Journal*, **11** (1), 41-83.

Nicholson, C., C. Sorlein, T. Atwater, J.C. Crowell, and B.P. Luyendyk (1994), Microplate capture, rotation of the western Transverse Ranges, and initiation of the San Andreas transform as a low-angle fault system, *Geology*, **22**, 491- 495.

O'Nions, R.K. and C.J. Ballentine (1993), Rare gas studies of basin scale fluid movement, *Phil. Trans. R. Soc. Lond. A*, **344**, 141-156.

O'Nions, R.K. and E.R. Oxburgh (1988), Helium volatile fluxes and the development of continental crust, *Earth Planetary Sci. Letters*, **90**, 331-347.

Oxburgh, E.R., R.K. O'Nions, and R.I. Hill (1986), Helium isotopes in sedimentary basins: *Nature*, **324**, 632-635.

Oxburgh, E.R., and R.K. O'Nions (1987), Helium loss, tectonics, and the terrestrial heat budget, *Science*, **237**, 1583-1588.

Person, M.A., and G. Garven (1992), Hydrologic constraints on petroleum generation within continental rift basins: theory and application to the Rhine Graben, *AAPG Bulletin*, **76**, 468-488.

Phillips, O.M. (1991), *Flow and Reactions in Permeable Rocks*, Cambridge University Press, New York, 285 p.

Polyak, B.G. and I.N. Tolstikhin (1985), Isotopic composition of the Earth's helium and the problem of the motive forces of tectogenesis, *Chemical Geology*, **52**, 9-33.

Porcelli, D. and T.R. Elliott (2008), The evolution of He isotopes in the convecting mantle and the preservation of high $^{3}He/^{4}He$ ratios, *Earth Planetary Sci. Letters*, **269** (1-2), 175-185.

Poreda, R.J., P.D. Jenden, I.R. Kaplan, and H. Craig (1986), Mantle helium in Sacramento basin natural gas wells, *Geochimica et Cosmochimica Acta*, **50**, 2847-2853.

Price, L.C., M. Pawlewicz, and T. Daws (1999), Organic Metamorphism in the California Basins, *U.S. Geological Survey Bulletin*, **2174-A**, 34 p.

Rice, J.R. (1992), Fault stress, pore pressure distribution, and the weakness of the San Andreas fault. In: *Fault Mechanics and Transport Properties of Rocks*, edited by Evans, B. and T.F. Wong, Academic Press, London, 475–503.

Romanyuk, T., W.D. Mooney, S. Detweiler (2007), Two lithospheric profiles across southern California derived from gravity and seismic data, *Journal of Geodynamics*, **43**, 274-307.

Sano, Y. and B. Marty (1995) Origin of carbon in fumarolic gas from island arcs, *Chemical Geology*, **119**, 265-274.

Schmandt, B., and R. Clayton (2013), Analysis of teleseismic P waves with a 5200-station array in Long Beach, California: Evidence for an abrupt boundary to Inner Borderland rifting, *Journal of Geophysical Research*, **118**, 1-19.

Shaw, J.H., and J. Suppe (1996), Earthquake hazards of active blind- thrust faults under the central Los Angeles basin, California, *Journal of Geophysical Research*, **101**, 8623-8642.

Torgersen, T. (1993), Defining the role of magmatism in extensional tectonics: helium 3 fluxes in extensional basins, *Journal of Geophysical Research*, **98**, 16257-16269.

Torgersen, T. and J. O'Donnell (1991), The degassing flux from the solid Earth--release by fracturing, *Geophysical Research Letters*, **18** (5), 951-954.

Umeda, K., K. Asamori, and T. Kusano (2013), Release of mantle and crustal helium from a fault following an inland earthquake, *Applied Geochemistry*, **37**, 134-141.

Umeda, K., G.F. McCrank, and A. Ninomiya (2007), Helium isotopes as geochemical indicators of a serpentized fore-arc mantle wedge, *Journal of Geophysical Research*, **112,** B10206, doi:10.1029/2007JB005031.

Umeda, K., and A. Ninomiya (2009), Helium isotopes as a tool for detecting concealed active faults,*Geochem.,Geophys.,Geosyst.*,**10**,Q08010. http://dx.doi.org/10.1029/2009GC002501.

van der Kamp, G. (1984), Evaluating the influence of groundwater flow systems on geothermal conditions. In: *Energy Developments: New Forms, Renewable, Conservation, Proceedings of Energex '84*, Regina, Saskatchewan, May 14-15, edited by F.A. Curtis, Pergamon Press, 297-301.

van der Kamp, G., and S. Bachu (1989), Use of dimensional analysis in the study of thermal effects of various hydrogeological regimes. In: *Hydrogeological Regimes and Their Subsurface Thermal Effects*, AGU Geophysical Monograph **47**, edited by Beck, A.E., G. Garven, and L. Stegena, 23-28.

Wallace, R.E. (ed.) (1990), The San Andreas Fault System, California, *USGS Prof. Paper*, **1515**, 304 p.

Welhan, J.A., R. Poreda, J.E. Lupton, and H. Craig (1979), Gas chemistry and helium isotopes at Cerro Prieto, *Geothermics*, **8**, 241-244.

Wiersberg, T. and J. Erzinger (2007), A helium isotope cross-section study through the San Andreas Fault at seismogenic depths, *Geochem., Geophys., Geosyst.*, **8**, 1-12.

Williams, C.F., L.A. Beyer, F.V. Grubb, and S. Galanis (2001), Heat flow and the seismotectonics of the Los Angeles and Ventura basins of Southern California, *Abstract #S11A-0534 presented at the 2001 Fall Meeting, AGU*, San Francisco, CA, Dec. 10-14.

Wright, T.L. (1991), Structural geology and tectonic evolution of the Los Angeles basin, In: *Active Margin Basins*, edited by Biddle, K.T., *AAPG Memoirs*, **52**, 35-134.